Geological Society of America
Special Paper 419
2007

Thermal evolution and exhumation of deep-level batholithic exposures, southernmost Sierra Nevada, California

J. Saleeby
K.A. Farley
Division of Geological and Planetary Sciences, California Institute of Technology, Pasadena, California

R.W. Kistler
R. Fleck
United States Geological Survey, Menlo Park, California

ABSTRACT

The Tehachapi complex lies at the southern end of the Sierra Nevada batholith adjacent to the Neogene-Quaternary Garlock fault. The complex is composed principally of high-pressure (8–10 kbar) Cretaceous batholithic rocks, and it represents the deepest exposed levels of a continuous oblique crustal section through the southern Sierra Nevada batholith. Over the southern ~100 km of this section, structural/petrologic continuity and geochronological data indicate that ≥35 km of felsic to intermediate-composition crust was generated by copious arc magmatism primarily between 105 and 99 Ma. In the Tehachapi complex, these batholithic rocks intrude and are bounded to the west by similar-composition gneissic-textured high-pressure batholithic rocks emplaced at ca. 115–110 Ma. This lower crustal complex is bounded below by a regional thrust system, which in Late Cretaceous time tectonically eroded the underlying mantle lithosphere, and in series displaced and underplated the Rand Schist subduction assemblage by low-angle slip from the outboard Franciscan trench. Geophysical and mantle xenolith studies indicate that the remnants of this shallow subduction thrust descend northward through the crust and into the mantle, leaving the mantle lithosphere intact beneath the greater Sierra Nevada batholith. This north-dipping regional structure records an inflection in the Farallon plate, which was segmented into a shallow subduction trajectory to the south and a normal steeper trajectory to the north.

We combine new and published data from a broad spectrum of thermochronometers that together form a coherent data array constraining the thermal evolution of the complex. Integration of these data with published thermobarometric and petrogenetic data also constrains the tectonically driven decompression and exhumation history of the complex. The timing of arc magmatic construction of the complex, as denoted above, is resolved by a large body of U/Pb zircon ages. High-confidence thermochronometric data track a single retrogressing path commencing from widely established solidus conditions at ca. 100 Ma, and traversing through time-temperature space as follows: (1) Sm/Nd garnet ~770–680 °C at ca. 102–95 Ma, (2) U/Pb titanite

Saleeby, J., Farley, K.A., Kistler, R.W., and Fleck, 2007, Thermal evolution and exhumation of deep-level batholithic exposures, southernmost Sierra Nevada, California, *in* Cloos, M., Carlson, W.D., Gilbert, M.C., Liou, J.G., and Sorensen, S.S., eds., Convergent Margin Terranes and Associated Regions: A Tribute to W.G. Ernst: Geological Society of America Special Paper 419, p. 39–66, doi: 10.1130/2007.2419(02).

~750–600 °C at ca. 102–95 Ma, (3) Ar/Ar hornblende ~570–490 °C at ca. 94–91 Ma, (4) Rb/Sr biotite ~390–260 °C at ca. 90–86 Ma, (5) Ar/Ar biotite ~320–240 °C at ca. 88–85 Ma, and (6) (U-Th)/He zircon ~230–170 °C at ca. 88–83 Ma. Additional stratigraphic constraints place the complex at surface conditions in Paleocene–early Eocene time (ca. 66–55 Ma).

Integration of these results with thermobarometric and structural data, including published data on the underlying Rand Schist, reveals a profound tectonic event whereby rapid cooling and exhumation at rates potentially as high as 100s °C/m.y. and >5 mm/yr initiated at ca. 98 Ma and peaked between 96 and 94 Ma. Between 93 and 85 Ma, cooling rates remained high, but decelerated with or without significant exhumation. Subsequent cooling and exhumation rates are poorly constrained but were much slower and ultimately resulted in Paleocene-Eocene surface exposure. Initial rapid exhumation and cooling are hypothesized to have been driven by abrupt flattening in the corresponding segment of the Farallon plate and the resulting tectonic erosion of the underlying mantle lithosphere. Protolith as well as metamorphic pressure-temperature and age constraints on the Rand Schist indicate its rapid low-angle subduction between 93 and 88 Ma. Comparison of the Rand Schist and Tehachapi complex pressure-temperature-time paths in conjunction with structural relations strongly suggest that the schist ascended the equivalent of ~4 kbar relative to the Tehachapi complex by low-angle normal displacement along the Rand fault between 88 and 80 Ma to attain its current underplated structural position. Such extensional tectonism is hypothesized to have been driven by slab rollback during the demise of the southern California region shallow slab segment.

Keywords: Sierra Nevada, thermochronology, rapid exhumation.

INTRODUCTION

Structurally continuous oblique sections into deep continental crust are important in that they provide opportunities to directly study the variations in composition and structure of the middle to lower crust. Such exposures by their existence pose important problems in tectonics and surface processes with respect to the mechanisms leading to their exposure. The absolute timing and rates of the exhumation of deep crustal sections are critical aspects of exploring such mechanisms. The pressure, temperature, and time relations recorded in the mineralogy, phase chemistry, and radiogenic isotopic systems of deeply exhumed crustal rocks are the keys to these temporal relations. In this study, we integrate published thermobarometric data with new data on an array of thermochronometers in order to constrain the thermal and exhumation history of the deepest exposed levels of an oblique crustal section through the southern Sierra Nevada batholith. The igneous history of these deep-level batholithic rocks has been relatively well constrained by field and petrographic studies, and by U/Pb zircon and Sr, Nd, Pb, and O isotopic studies (Saleeby et al., 1987; Ross, 1989; Kistler and Ross, 1990; Pickett and Saleeby, 1994; Lackey et al., 2005). These studies in conjunction with thermobarometric data (Ague and Brimhall, 1988; Pickett and Saleeby, 1993; Ague, 1997) provide a well-defined initial state for the study of the subsequent cooling, decompression, and exhumation of the deep-level rocks.

In this study, we focus on the radiogenic isotopic systems of U/Pb titanite, Sm/Nd garnet, Ar/Ar hornblende and biotite, Rb/Sr biotite, and (U-Th)/He zircon, which provide thermochronometric datums in the temperature range of ~700 to ~180 °C (Harrison, 1981; Elphick et al., 1985; Cherniak, 1993; Dahl, 1997; Ganguly et al., 1998; McDougall and Harrison, 1999; Fleck et al., 2002; Reiners et al., 2004). Additional low-temperature constraints are provided by published fission track and (U-Th)/He apatite data (Naeser et al., 1990; Niemi et al., 2004), and by stratigraphic relations (Cox, 1987; Nilsen, 1987). We thus have an opportunity to track the cooling and exhumation history of the deep batholithic rocks over a depth interval that spans the site of petrogenesis to surface exposure.

Regional geologic relations show that this exhumation history is unique to the southern end of the Sierra Nevada batholith, which for much of its ~600 km length to the north has only been exhumed to relatively shallow levels (Evernden and Kistler, 1970; Ague and Brimhall, 1988). In that the deeply exhumed rocks are in structural continuity with the greater Sierra Nevada batholith to the north, such deep exhumation in the south has rendered an oblique crustal section through nearly the entire arc-generated crust (Saleeby et al., 2003). These deeply exhumed rocks mark a critical tectonic boundary in the southwestern Cordilleran batholithic belt in that they coincide with the transition of a coherent zone in the belt and its adjacent forearc basin to the north, and a highly disrupted and dispersed zone to the south. The thermal and exhumation history of this zone are critical for the interpreta-

tion of this profound change in batholithic belt structure. In the discussions below, exhumation is used to denote the displacement of rocks with respect to Earth's surface where the rate of exhumation is the total rate of erosion and tectonic denudation (after England and Molnar, 1990).

GEOLOGIC SETTING

Regional Relations

The Sierra Nevada batholith is the most intensely studied segment of the North American Cordilleran batholithic belt. It extends for an ~600 km strike length in the central California region, having formed principally in Cretaceous time (Evernden and Kistler, 1970). It is unique relative to most of the Cordilleran batholithic belt in that for most of its length it is still in tectonic continuity with its forearc basin (Great Valley) as well as the subduction accretion assemblage (Franciscan Complex) that records its plate-tectonic-related genesis. For most of its length, the Sierra Nevada batholith is exposed over the relatively shallow crustal range of ~5–12 km (Evernden and Kistler, 1970, p. 12–14; Ague and Brimhall, 1988). As shown in the Figure 1 inset, however, over its southern ~100 km there is a continuous gradient in depth of exposure along which broadly coeval middle Cretaceous shallow-level batholithic rocks grade into exposures as deep as ~35 km (Pickett and Saleeby, 1993). The deep-level exposures occur in a transverse zone that trends across the regional northwest trend of the batholith and that constitutes the physiographically anomalous Tehachapi Range (Fig. 1). The southern margin of the Tehachapi Range is bounded by the Neogene-Quaternary Garlock fault, which forms the boundary between the coupled Sierran–Great Valley tectonic province to the north, and the Mojave Desert and Transverse Ranges to the south. Perhaps more fundamental, however, is that the Tehachapi Range coincides with a Late Cretaceous transverse structural boundary south of which an ~500 km long segment of the batholithic belt and its adjacent forearc basin is tectonically disrupted (Malin et al., 1995). The disrupted batholithic rocks include those of the western Mojave Desert and the Salinia and the San Gabriel terranes, which have been offset ~320 km along the San Andreas fault (Fig. 1 inset). The initial and principal stages of such batholithic belt disruption are linked to the same Late Cretaceous regional tectonic event that led to the deep-level exposures of the Tehachapi Range (Saleeby, 2003). These deep-level rocks are informally referred to as the Tehachapi complex, although it is emphasized that this complex is in structural continuity with the greater Sierra Nevada batholith to the north, and that it shares a common petrogenetic framework with the greater Sierra Nevada batholith.

The Tehachapi complex is also unique relative to the rest of the Sierra Nevada batholith to the north in that it is truncated at depth by a regional thrust system (Rand fault) that underplated Franciscan-affinity subduction accretion assemblages directly beneath the batholith (Malin et al., 1995; Saleeby, 2003). This thrusting event also disrupted the southern Great Valley forearc basin and drove the deep exhumation of the complex. Remnants of the thrust system and underplated subduction assemblages are also preserved along the base of disrupted batholithic complexes of the Mojave Desert and Transverse Ranges to the south (Jacobson et al., 1996; Barth and Schneiderman, 1996). The underplated rocks constitute a family of distinct high- to intermediate-*P/T* schists locally named the Rand Schist in the Tehachapi–northern Mojave Desert region. The structural position of these schists, relative to more typical Franciscan assemblages, and the destruction of the corresponding forearc basin indicate a minimum downdip displacement of ~100 km along a low-dipping subduction trajectory. Estimates of pressures and temperatures of equilibration for the Rand Schist, relative to those of more typical Franciscan high-*P/T* metamorphic units, further suggest emplacement of the schist along a lower-dipping subduction trajectory and also under higher shear stress conditions than the Franciscan units (Peacock, 1992; Pickett and Saleeby, 1993; Jacobson, 1995).

The regional structural relations of the Rand and related schists indicate that the mantle lithosphere underpinnings for the southernmost Sierra Nevada batholith and adjacent batholithic belt to the south have been tectonically removed. In contrast, petrogenetic studies of lower crust–upper mantle xenoliths that were entrained in Neogene volcanic rocks erupted through the greater Sierra Nevada batholith to the north indicate that the mantle lithosphere that formed beneath the batholith remained intact to the north, thereby indicating the lack of such lithosphere-scale (Rand) thrusting to the north (Ducea and Saleeby, 1996, 1998; Saleeby et al., 2003). Such north to south contrasts in the lower crust–upper mantle structure of the batholithic belt have been attributed to the Late Cretaceous segmentation of the Farallon plate into northern steeply dipping and southern shallowly dipping domains as it subducted beneath the southwestern Cordillera (Malin et al., 1995; Saleeby, 2003). The Tehachapi complex is hypothesized to have sat above the inflection in the segmented Farallon slab. The segmentation of subducting slabs into shallow flat and steeper normal domains is a well-documented phenomenon in active subduction-arc systems (Barazangi and Isacks, 1976; Gutscher et al., 2000). Little is known about the deep crustal response within magmatic arcs along the inflection zones between deep and shallow slab segments. The southern Sierra Nevada batholith oblique crustal section offers a glimpse into such a deep crustal tectonic system, and the thermochronologic and exhumation history discussed in this study offers some insights into this important class of problems.

Tehachapi Complex Nomenclature and Structural Relations

A generalized geologic map of the Tehachapi complex is shown with the thermochronometric sample sites in Figure 1. The Tehachapi complex consists of three principal rock suites: (1) Early Cretaceous (ca. 115–110 Ma) tonalitic gneiss with variable amounts of amphibolitic gabbro-diorite, and granodioritic gneiss; (2) pre-Cretaceous (protolith age) migmatitic paragneiss, derived from pelite-psammite, subordinate quartzite, calc-silicate gneiss

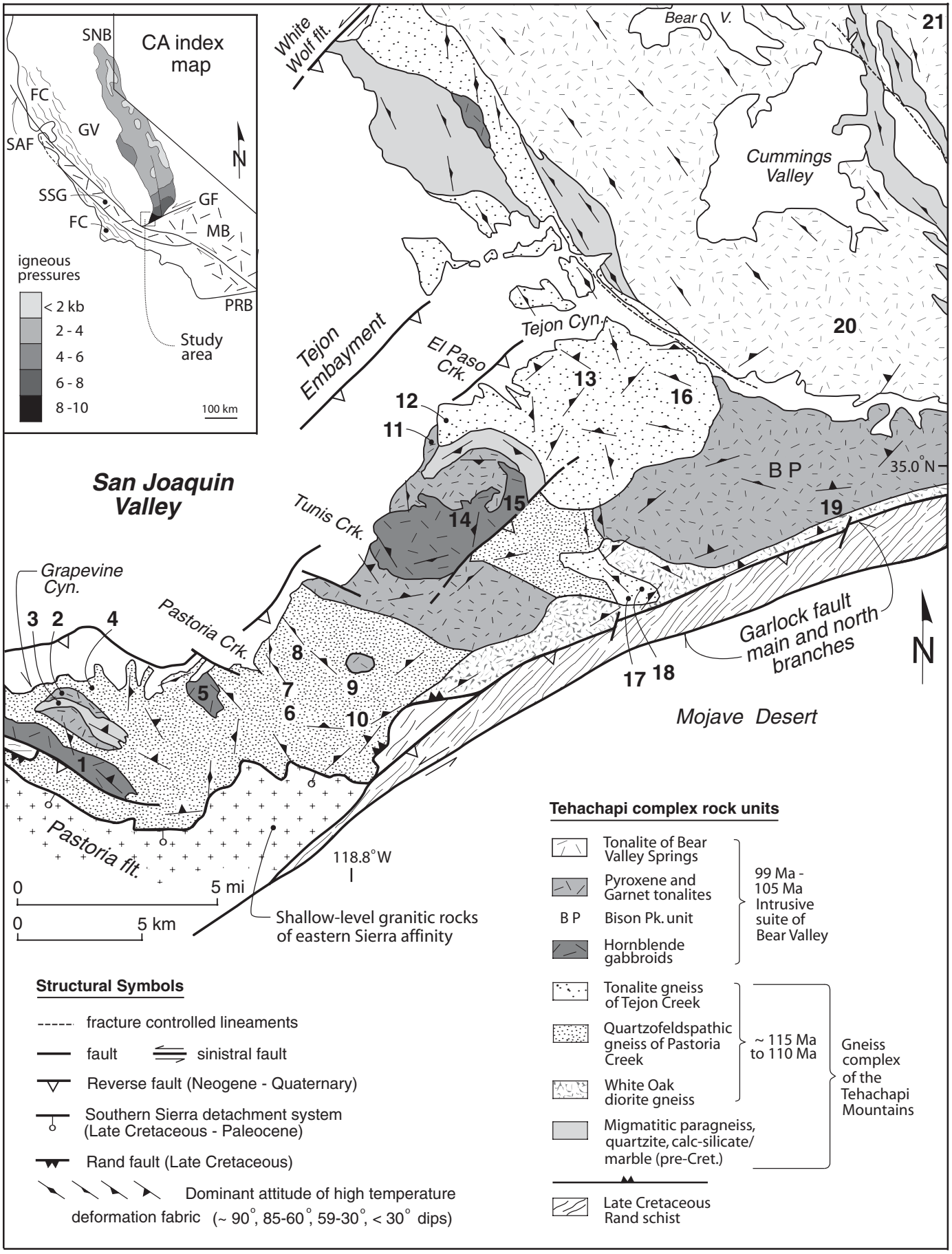
CA index map
SNB
FC
GV
SAF
SSG
GF
FC
MB
PRB
N
igneous pressures
< 2 kb
2 - 4
4 - 6
6 - 8
8 -10
Study area
100 km
White Wolf flt.
Bear V.
21
Cummings Valley
20
Tejon Embayment
El Paso Crk.
Tejon Cyn.
12
11
13
16
B P
35.0°N
San Joaquin Valley
Tunis Crk.
14
15
19
Grapevine Cyn.
3
2
4
Pastoria Crk.
8
7
6
9
10
5
1
17
18
Garlock fault main and north branches
N
Mojave Desert
Pastoria flt.
118.8°W
0
5 mi
0
5 km
Shallow-level granitic rocks of eastern Sierra affinity
Tehachapi complex rock units
Tonalite of Bear Valley Springs
Pyroxene and Garnet tonalites
B P Bison Pk. unit
Hornblende gabbroids
99 Ma - 105 Ma Intrusive suite of Bear Valley
Tonalite gneiss of Tejon Creek
Quartzofeldspathic gneiss of Pastoria Creek
White Oak diorite gneiss
~ 115 Ma to 110 Ma
Migmatitic paragneiss, quartzite, calc-silicate/ marble (pre-Cret.)
Gneiss complex of the Tehachapi Mountains
Late Cretaceous Rand schist
Structural Symbols
fracture controlled lineaments
fault
sinistral fault
Reverse fault (Neogene - Quaternary)
Southern Sierra detachment system (Late Cretaceous - Paleocene)
Rand fault (Late Cretaceous)
Dominant attitude of high temperature deformation fabric (~ 90°, 85-60°, 59-30°, < 30° dips)

with sparse marble; and (3) middle Cretaceous (ca. 105–99 Ma) tonalitic, dioritic, gabbroic, and subordinate granodioritic intrusives (Saleeby et al., 1987; Sams and Saleeby, 1988; Ross, 1989). The Early Cretaceous orthogneisses and their paragneiss enclaves are informally named the gneiss complex of the Tehachapi Range. These are also referred to as the Tehachapi gneisses, or gneisses, and in the case of strictly igneous protoliths, orthogneisses. The orthogneisses consist of three informal units: (1) the quartzofeldspathic gneiss of Pastoria Creek, (2) the tonalite gneiss of Tejon Creek, and (3) the White Oak diorite gneiss. The Pastoria Creek unit is lithologically the most variable with abundant tonalite and mafic rock, but also appreciable granodiorite. It is modestly to strongly layered. The Tejon Creek unit is more homogeneous, being predominately tonalite, and its local layering reflects mainly deformed commingled and disrupted mafic intrusives. The White Oak unit is a tectonic unit that lies along the structural base of the complex. Its protolith is principally dioritic, although it also contains appreciable tonalite. It is characterized by numerous mylonite zones that are superimposed over the higher-temperature gneissic fabrics, and also zones of intense retrograding to chloritic schists, cataclasite, and tectonic breccia.

The middle Cretaceous intrusives are informally named the intrusive suite of Bear Valley. These are also referred to as the Bear Valley suite, or Bear Valley intrusives. These intrusives include the tonalite of Bear Valley Springs, a batholith-scale pluton that extends for ~100 km north of the Tehachapi Range area and for an appreciable distance within the adjacent San Joaquin Valley subsurface (Ross, 1979). Only the southern ~30 km of the Bear Valley Springs pluton is included in the Tehachapi complex. Physiographically, this includes the pluton as exposed in the Tehachapi Range, which encompasses its deeper exposed levels (>6 kbar). At its deepest exposed levels, the Bear Valley Springs pluton grades into the hypersthene tonalite of Bison Peak (BP on Fig. 1). Similar hypersthene, and two-pyroxene (± biotite ± hornblende) tonalites as well as garnet tonalites of the Bear Valley suite occur as isolated intrusions within the gneisses. In the lower Tunis Creek area, Bison Peak–like pyroxene tonalites finger through the gneisses in a fashion that is too complex to show at the scale of Figure 1. Bear Valley intrusives within the gneisses also include the three mappable gabbroic cumulate bodies of the lower Tunis and Pastoria Creek areas and the Grapevine Canyon area.

The orthogneisses are in most areas readily distinguished from the Bear Valley suite by near-pervasive ductile deformation fabrics, which in most locations represent deformation under high-temperature solidus to hot subsolidus conditions. Bear Valley suite rocks locally take on gneissic fabrics developed under similar high-temperature conditions, and in some locations distinction from their orthogneiss host is difficult. The Bear Valley suite gabbros commonly preserve cumulate layering and textures, and only locally exhibit ductile deformation features. An important structural feature of these gabbros is common domains of partial melting and the development of migmatite. Coarse garnet growth as a residual melanosome phase characterizes such migmatites, and the derivative leucosomes commonly occur as felsic halos and lenses around the residual garnets. Localized brittle fracturing during garnet growth and related low-volume partial melting is a common feature of the migmatite domains. Such fracture systems served both as conduits for leucosome migration and as pathways for pegmatite dike emplacement.

Major tectonic breaks affecting the Tehachapi complex appear to be restricted to the Rand fault, which truncates the base of the complex, and the late Neogene–Quaternary Garlock fault, which has displaced the complex by ~50 km of sinistral slip from broadly correlative rocks of the northern Mojave Desert (Malin et al., 1995). Also shown on Figure 1 is the Pastoria fault, which is interpreted as a member of the Late Cretaceous–Paleocene southern Sierra detachment system, a low-angle normal fault system that is in part responsible for the deep exhumation of the complex (Wood and Saleeby, 1998; Saleeby, 2003). The Pastoria fault places relatively high-level eastern Sierra Nevada batholith–affinity batholithic rocks above the Tehachapi complex. Late Neogene–Quaternary north-directed reverse and/or sinistral faults, and open flexural folds, also affect the complex but do not produce major disruptions (Ross, 1989; Malin et al., 1995; Saleeby and Foster, 2004). The large variations in the attitudes of the high-temperature deformation fabrics between the Tejon Creek and Grapevine Canyon areas as well as the complex map trace of the Pastoria fault reflect the late-stage flexural folding of the complex (Fig. 1). One important result of these superimposed structures is the local development of sufficient structural relief to lead to the Holocene erosional exhumation of the Rand Schist over areas of structural culmination. The two largest of such structural culminations are mappable half windows into the schist along the north branch of the Garlock fault near longitude 188.8°W, and along the west margin of Figure 1 in the Grapevine Canyon area. Early workers in the region mapped a high-angle fault along a strong topographic lineament that coincides with Tejon Canyon. Neither our mapping nor Ross's (1989) showed evidence for a fault surface or any evidence for fault truncation of lithologic units. Nevertheless, strong, evenly spaced fracture sets control the lineament, and these appear to represent distributed brittle fracture along the Bear Valley Springs pluton–Tejon Creek gneiss contact zone and may be important in reconciling some of the aberrant lower-temperature data. Late Cretaceous to Neogene clockwise rotation of as much as ~45° also affected the com-

Figure 1. Generalized geologic map of the western Tehachapi Range showing thermochronometric sample locations. Geology after Sharry (1981), Saleeby et al. (1987), Sams and Saleeby (1988), Ross (1989), Pickett and Saleeby (1993), and Saleeby and Foster (2004). Inset shows outline of Sierra Nevada batholith (SNB) with contours of igneous emplacement pressures after Ague and Brimhall (1988) and Pickett and Saleeby (1993). FC—Franciscan Complex; GF—Garlock fault; GV—Great Valley; MB—Mojave batholith; PRB—Peninsular Ranges batholith; SAF—San Andreas fault; SSG—Salinia–San Gabriel batholithic terrane displaced from southern California region.

plex (Kanter and McWilliams, 1982). Such basement rotation dies out in and north of the Bear Valley area (Fig. 1).

The Tehachapi complex may be divided into four structural domains based on both primary and superimposed structural relations. These consist of (1) a western domain lying in the Pastoria Creek–Grapevine Creek area, (2) an eastern domain lying in the Tunis Creek–Tejon Creek area, (3) a basal domain lying proximal to the Rand fault, and (4) the deeper levels of the Bear Valley Springs pluton. The domain boundaries are transitional. The western and eastern domains are distinguished from one another by a higher proportion of Bear Valley intrusives relative to gneiss host rocks within the eastern domain (Fig. 1). The basal domain lies along the north branch of the Garlock fault encompassing much of the White Oak diorite gneiss. This domain is defined by structural position and by the tectonic overprint discussed above as being characteristic of the White Oak unit. This overprint is related to the Rand fault, which is shown by mapping and seismic reflection data to lie at shallow levels beneath the basal domain (Malin et al., 1995; Saleeby and Foster, 2004). Reverse slip on the north branch of the Garlock fault has displaced the tectonically underlying schist up against the basal domain at the current level of exposure. The superimposed mylonite zones that characterize the basal domain also occur as discrete high-strain zones throughout various parts of the complex, but such zones appear to be restricted in both the extent and the degree of disruption of primary structure.

REVIEW OF GEOCHRONOLOGIC AND THERMOBAROMETRIC DATA

Throughout the ~600 km length of the Sierra Nevada batholith, Cretaceous magmatism is shown to have commenced between ca. 140 Ma and 130 Ma along its western margin with minimal or no recycled continental components. Magmatism progressed eastward through much of Cretaceous time with increasing contributions from continental reservoirs (Kistler and Peterman, 1973; DePaolo, 1981; Kistler, 1990; Chen and Tilton, 1991; Pickett and Saleeby, 1994; Coleman and Glazner, 1998; Ducea, 2001). This regional pattern in batholith zonation is reflected in initial Sr, Pb, and Nd isotopic composition patterns, pluton ages, bulk composition patterns, and also metamorphic framework assemblages. Coupled variations in these parameters render longitudinal internal belts that are regionally continuous and that extend along the Cordilleran batholithic belt well beyond the limits of the Sierra Nevada batholith. The Tehachapi complex lies within the western (Early to middle Cretaceous) domain of this regional pattern. U/Pb zircon ages on all major intrusive units of the complex indicate high-volume magmatism at ca. 115–110 Ma and ca. 105–99 Ma (Saleeby et al., 1987; Pickett and Saleeby, 1994; GSA Data Repository).[1] Batholithic rocks as old as ca. 130 Ma occur to the west of the study area, and the Tehachapi complex is bounded to the east by a large granodioritic pluton of ca. 90 Ma (Saleeby et al., 1987; James, 1992). Throughout much of the Sierra Nevada batholith, Cretaceous magmatism is shown to have migrated eastward through time (Evernden and Kistler, 1970), with a high-density array of U/Pb zircon data along a corridor between latitudes 36°N and 37°N yielding an integrated rate of ~3 mm/yr (Saleeby and Sharp, 1980; Chen and Moore, 1982; Saleeby et al., 1990).

The southern Sierra Nevada batholith oblique crustal section extends from volcanic and subvolcanic pluton levels in the north to deep batholithic levels of the Tehachapi complex in the south (Saleeby and Busby-Spera, 1986; Ague and Brimhall, 1988; Saleeby, 1990). Estimates of igneous emplacement pressures for the Tehachapi complex based on Al in hornblende (Hammarstrom and Zen, 1986; Hollister et al., 1987) show that the regional trend of progressively higher igneous crystallization pressures continues southward through the Bear Valley Springs pluton and into the complex where pressures of 7.8–9.3 kbar prevail (Pickett and Saleeby, 1993). Samples for which these pressure determinations were made contain the complete buffering mineral assemblage, and the results have been corroborated by thermodynamically based pressure determinations (Ague, 1997). These data have not been further manipulated by the techniques of Anderson and Smith (1995), which result in pressure changes that lie within the uncertainty of the technique. Quantitative thermobarometry for the complex based on garnet-plagioclase-quartz-hornblende (or -biotite) yield a clustering of minimum estimates at 7.1–10.8 kbar and 690–790 °C (Pickett and Saleeby, 1993). This work further shows (1) the occurrence of kyanite in pelitic restite lenses of garnet tonalite indicating minimum conditions of ~7.6 kbar and ~690 °C; (2) additional quantitative thermobarometric determinations with values as high as ~950 °C and ~17 kbar in the western domain, and an ~5 km^2 area in the eastern domain that reequilibrated at ~4 kbar and ~600 °C; and (3) quantitative thermobarometric determinations for the peak conditions in the adjacent Rand Schist of ~8.2–9.7 kbar and ~590–680 °C.

Rapid exhumation of the Tehachapi complex as well as the tectonically underplated Rand Schist is indicated by tectonic truncations along the base of a Late Cretaceous–Paleocene detachment system, which places relatively shallow-level eastern Sierra Nevada batholithic and associated metamorphic framework assemblages onto both the Tehachapi complex and the schist (Wood and Saleeby, 1998; Saleeby and Foster, 2004). These are nonconformably overlain by middle Paleocene through Eocene locally derived marine clastic strata (Cox, 1987; Nilsen, 1987). Thus middle Cretaceous deep batholithic conditions were terminated in the Late Cretaceous in conjunction with schist underplating and high-magnitude extensional faulting, and by the beginning of the Cenozoic the entire deep crustal complex was exposed and nonconformably overlapped under marine conditions. The thermal evolution of this complex from deep-level solidus to surface conditions in relation to the driving tectonics is the primary focus of this paper.

[1]GSA Data Repository item 2007067, substantial text module, is available on the Web at http://www.geosociety.org/pubs/ft2007.htm. Requests may also be sent to editing@geosociety.org.

DATA OVERVIEW

We present new data that track the thermochronologic evolution of the Tehachapi complex from near-pervasive solidus conditions to relatively low-temperature (~180 °C) conditions. The temperature ranges used for the different thermochronometric systems are summarized in Table 1. New data are presented in Tables 2–5 for U/Pb titanite, Sm/Nd garnet, Ar/Ar-Rb/Sr hornblende-biotite, and (U-Th)/He zircon respectively. Table 6 summarizes the different age determinations and coupled thermobarometric data. Analytical procedures and information on sample locations, petrography, and relations with samples for which isotopic and thermobarometric data have been published elsewhere are presented in the GSA Data Repository. In this section, a brief overview of the different data sets is presented, and then in the following section, the different data sets are integrated into a thermochronologic analysis.

One of the principal conclusions of this paper is that the thermochronometers track a single rapid retrogressing path commencing at a ca. 100 Ma *P-T* maximum established by copious deep-level arc magmatism. The timing of the initial *P-T* maxima is established by U/Pb zircon ages on every major intrusive unit of the complex that has been thus far recognized by field and petrographic studies (Saleeby et al., 1987; Pickett and Saleeby, 1994; GSA Data Repository). To better constrain the temporal relations of these initial peak conditions, select U/Pb titanite and Sm/Nd garnet ages were determined. The titanite ages were determined on several orthogneiss samples as a test of how extensive lower crustal reheating was in the ca. 115–110 Ma orthogneisses as a result of voluminous ca. 105–99 Ma magmatism. The Sm/Nd garnet ages were determined at key locations as a temporal index for the garnet-based thermobarometric data, and also to better constrain the temporal relations of low-volume partial remelting that was widespread in the complex. Structural and textural relations also indicate that such low-volume remelting mark the terminal phases of the peak magmatic and thermal conditions. These relations are of general petrologic interest in that zones of hornblende granulite facies rocks are related to the domainal remelting, and such granulitic rocks are interpreted as the types of materials that may form as residues in the production of felsic batholiths (White and Chappell, 1977; Rapp et al., 1991; Ducea, 2001). It is asserted that the petrologic record of such granulitic conditions are merely "footprints" in a retrogressive *P-T* path commencing with wet basalt and tonalite solidus conditions. These "footprints" were frozen into the deep-level batholithic rocks by rapid cooling and exhumation related to the tectonics of schist underplating.

TABLE 1. TEMPERATURE RANGES USED FOR INTERPRETATION OF THERMOCHRONOMETERS

System	*T* range (°C)	Source/notes
U/Pb zircon (Bear Valley suite and orthogneisses)	800–875	Watson and Harrison (1984) zircon solubility modeling and Tehachapi complex elemental concentration data (Pickett, 1991)
U/Pb zircon (pegmatite dikes)	625–725	Water-saturated liquidus and solidus surfaces at ~10 kbar (Johnston and Wyllie, 1988; Van der Laan and Wyllie, 1992)
Sm/Nd garnet	580–750	Pickett and Saleeby (1993) thermometry and comparable diffusivities of Sm, Nd, and major cations (Elphick et al., 1985; Ganguly et al., 1998)
U/Pb titanite	500–700	Cherniak (1993), Dahl (1997)
Ar/Ar hornblende	490–570	Harrison (1981)
Rb/Sr biotite	255–395	McDougall and Harrison (1999), Fleck et al. (2002)
Ar/Ar biotite	240–320	McDougall and Harrison (1999)
(U-Th)/He zircon	170–190 and 190–220	Reiners et al. (2004) with range extended for ~100 °C/m.y. cooling rates (Dodson, 1973)
Fission track zircon	160–250	Naeser et al. (1990)
Fission track apatite	105–150	Naeser et al. (1990)
(U-Th)/He apatite	63–73	Farley (2000)

TABLE 2. U/Pb TITANITE DATA FOR TEHACHAPI COMPLEX ORTHOGNEISSES §

Sample	Fraction† (μm)	Amount analyzed (mg)	^{238}U (ppm)	$^{206}Pb^*$ (ppm)	$\frac{^{206}Pb}{^{204}Pb}$	$\frac{^{206}Pb^*}{^{238}U}$	$\frac{^{207}Pb^*}{^{206}Pb^*}$	$\frac{^{206}Pb^*}{^{238}U}$ age (Ma)	U/Pb zircon age (Ma)
4	200–250	7.2	133	1.78	249	0.01551	0.04858(27)	99.2 ± 0.9	113.5 ± 1.5
4	150–200	6.7	151	2.02	198	0.01546	0.04824(33)	98.9 ± 1.0	"
7	200–250	9.3	101	1.40	167	0.01597	0.04855(39)	102.1 ± 1.1	112.0 ± 1.5
12	200–250	8.3	143	1.87	211	0.01508	0.04811(29)	96.5 ± 1.3	110.5 ± 1.0
12	150–200	9.9	178	2.31	295	0.01499	0.04867(35)	95.9 ± 0.9	"
13	150–200	7.9	222	2.91	391	0.01516	0.04853(22)	97.0 ± 1.0	116.5 ± 1.5
16	200–250	10.2	298	3.83	427	0.01486	0.04806(19)	95.1 ± 0.9	111.5 ± 1.5

Notes: Decay constants used in age calculations: $\lambda^{238}U = 1.55125 \times 10^{-10}$ yr^{-1} and $\lambda^{235}U = 9.8485 \times 10^{-10}$ yr^{-1} (Jaffey et al., 1971). $^{238}U/^{235}U$ atom = 137.88. Uncertainties at 95% confidence level, and for $^{207}Pb^*/^{206}Pb^*$ are given as ± in last two figures. U/Pb zircon ages are from Saleeby et al. (1987) and GSA Data Repository.

†Samples handpicked to 99.9% purity prior to dissolution. Dissolution and chemical extraction techniques given in GSA Data Repository.

*Radiogenic; nonradiogenic correction based on 40 picogram blank Pb (1:18.78:15.61:38.50) and initial Pb (1:18.82:15.65:38.65) after Pickett and Saleeby (1994).

TABLE 3. Sm/Nd GARNET-MATRIX AGE DATA

Sample	System	Sm (ppm)	Nd (ppm)	$\frac{^{147}Sm}{^{144}Nd}$[1]	$\frac{^{143}Nd}{Nd}$[2]	Age (Ma)[3]
1	Leucosome matrix	4.95	26.32	0.114	0.512627 ± 13	-
1	Garnet	2.54	1.21	1.273	0.513361 ± 12	96.8 ± 2.9
2	Rock matrix	3.19	18.77	0.103	0.512778 ± 15	-
2	Garnet	2.09	1.55	0.817	0.513240 ± 14	99.0 ± 3.1
5	Leucosome matrix	5.67	44.06	0.078	0.512725 ± 15	-
5	Garnet	3.11	1.80	1.049	0.513431 ± 13	95.9 ± 3.0
6b	Rock matrix	6.01	28.91	0.126	0.512741 ± 12	-
6b	Garnet	2.93	1.94	0.917	0.513270 ± 13	102.2 ± 2.9
15	Leucosome matrix	4.62	29.47	0.095	0.512618 ± 11	-
15	Garnet	2.21	1.02	1.314	0.513374 ± 13	94.8 ± 2.7

[1]Uncertainty of $^{147}Sm/^{144}Nd \oplus 0.3\%$.
[2]Nd isotopic ratios normalized to $^{146}Nd/^{144}Nd = 0.7219$; uncertainties in $^{143}Nd/^{144}Nd$ are standard errors.
[3]$\lambda^{147}Sm = 6.54 \times 10^{-12}$ yr^{-1}.
Analytical procedures given in GSA Data Repository.

TABLE 4. Rb/Sr AND Ar/Ar AGE DATA FOR BIOTITE AND HORNBLENDE (AGES IN Ma)

Sample	System	Rb (ppm)	Sr (ppm)	$^{87}Rb/^{86}Sr$	$^{87}Sr/^{86}Sr$	Sr_i	Rb/Sr age[†] (Ma)	$^{40}Ar/^{36}Ar$–$^{39}Ar/^{36}Ar$ isochron age (Ma)	$^{40}Ar/^{39}Ar$ total fusion age (Ma)	$^{40}Ar/^{39}Ar$ plateau age (Ma)
3	wr	96.3	211.1	1.320	0.70929	0.70740	-	-	-	-
3	bi	314.69	8.69	106.14	0.8395	0.70765	87.64 ± 1.1	87.2 ± 1.1	86.3	86.75 ± 0.24
4	bi	199	31.07	18.55	0.72913	0.70606[‡]	87.5 ± 1.1	-	-	-
6	wr	0.54	507	0.0032	0.70468	0.70468	-	-	-	-
6	bi	295.1	39.14	21.80	0.73228	0.70468	89.1 ± 1.2	-	-	-
6	hb	-	-	-	-	-	-	92.0 ± 1.7	91.7	91.35 ± 0.67
6b	hb	3.34	61.19	0.158	0.70434	0.70408	-	94.4 ± 1.9	92.9	93.67 ± 0.78
7	wr	50.5	279	0.523	0.70569	0.70484	-	-	-	-
7	hb	2.94	41.47	0.206	0.70481	0.70447	-	95.3 ± 1.8	93.8	94.68 ± 0.64
7	bi	321.4	28.69	32.41	0.74513	0.70504	87.0 ± 1.1	86.6 ± 4.1	83.0	85.13 ± 0.48
9	bi	93.4	25.74	10.51	0.71834	0.70502[‡]	89.2 ± 1.1	-	-	-
11	wr	49.6	316	0.454	0.70558	0.70493	-	-	-	-
11	bi	376.97	18.62	58.97	0.77783	0.70502	86.9 ± 1.3	88.5 ± 1.1	86.8	88.00 ± 34
12	wr	43.6	279	0.451	0.70614	0.70560	-	-	-	-
12	bi	390.69	26.32	43.17	0.75718	0.70560	84.1 ± 1.3	84.2 ± 2.6	87.5	88.02 ± 0.27
12	hb	-	-	-	-	-	-	94.8 ± 2.2	92.8	93.81 ± 0.86
13	bi	121	29.22	11.99	0.72001	0.70526[‡]	86.6 ± 1.1	-	-	-
16	wr	108	201	1.56	0.70699	0.70446	-	-	-	-
16	bi	698.1	12.22	168.53	0.90637	0.70513	84.0 ± 1.3	78.3 ± 1.8	80.6	80.50 ± 0.27
17a	wr	19.2	328	0.168	0.70457	0.70436	-	-	-	-
17a	bi	425.2	27.12	45.37	0.76012	0.70436	86.5 ± 1.2	87.4 ± 1.7	83.3	85.13 ± 0.48
17b	hb	6.09	57.01	0.309	0.70471	0.70421	-	93.0 ± 1.7	93.0	93.02 ± 0.57
17c	hb	52.57	118.4	1.284	0.7654	0.70520	-	88.4 ± 1.9	90.7	88.55 ± 0.
17c	bi	349.52	54.78	18.49	0.72450	0.70520	73.5 ± 1.0	81.4 ± 3.4	82.0	none
18	bi	96.1	15.99	17.39	0.72581	0.70500[‡]	84.2 ± 1.1	-	-	-
19	wr	28.8	351.2	0.236	0.70498	0.70465	-	-	-	-
19	bi	349	21.32	47.34	0.76024	0.70470	82.4 ± 1.0	-	-	-
20	bi	215	21.02	29.63	0.74267	0.70681[‡]	84.9 ± 1.5	-	-	-
21	wr	101	175	1.66	0.70739	0.70502	-	-	-	-
21	hb	15.34	14.74	3.01	0.70908	0.70531	88.1 ± 1.5	84.6 ± 1.5	85.4	85.21 ± 0.44
21	bi	513.47	17.22	87.04	0.79872	0.70573	75.2 ± 1.1	82.8 ± 1.1	78.4	81.64 ± 0.31

Note: bi—biotite, hb—hornblende, wr—whole rock.
[†]Mineral/whole-rock isochron age.
[‡]Sr_i wr data from Saleeby et al. (1987).

The western and eastern domains of the complex constitute its chief exposures and are considered to a first order to be structurally intact. These domains were the focus of our sampling (Fig. 1). To better constrain the thermal conditions and temporal relations of schist underplating, a series of samples was also taken from the basal domain. This included a relatively "pristine" mylonite zone (sample 17c) from the sample 17 site in the Tejon Creek unit proximal to the White Oak unit. This particular mylonite was chosen for its relative lack of retrograde mineral growth, which commonly plagues rocks of the complex with mylonitic overprints. Two samples are also included from the Bear Valley Springs pluton. These span igneous pressures of ~8–6.9 kbar and are tied to the regional pressure gradient that defines the southern end of the oblique crustal section (Fig. 1).

U/Pb Data

U/Pb zircon ages for the Tehachapi complex fall into three groups: (1) ca. 115–110 Ma orthogneisses, (2) ca. 105–99 Ma Bear Valley suite of intrusives, and (3) ca. 98–95 Ma pegmatite dikes. A number of the orthogneiss samples show modest degrees of age discordance interpreted to reflect mainly inheritance of early Paleo-

TABLE 5. (U-Th)/He ZIRCON AGE DATA

Sample	Age corrected (Ma)	U† (ppm)	Th† (ppm)	He (nmol/g)	Ft‡	Mean age (Ma)	2σ	MSWD (2σ)	%
4	89.11578	227.2123	32.17508	96.30272	0.839384	86.0	±2.5	2.5	2.90
4	86.58508	315.2301	59.66178	130.1759	0.832987				
4	82.49177	213.7395	48.45461	84.64584	0.831878				
4	86.25581	330.6318	76.84918	136.1176	0.82567				
8	64.77759	1053.867	1163.323	402.0435	0.855699	87.5	±3.5	5.5	6.30
8	87.79203	981.6888	276.4141	433.6368	0.860906				
8	81.12016	1410.743	179.2173	545.9512	0.845457				
8	87.05732	989.89	214.5463	431.6111	0.86936				
8	93.39998	1554.803	88.88688	683.0235	0.845814				
8	86.17686	305.1595	64.49503	129.3861	0.855126				
8	90.28484	1629.731	145.2439	684.3178	0.830532				
9	77.04646	670.218	80.83152	249.9983	0.85962	91.1	±7.7	18	20
9	79.08343	494.1944	121.1419	197.2377	0.871247				
9	91.05411	509.0096	133.5293	233.4222	0.865084				
9	93.4392	509.4136	163.672	239.7074	0.853737				
9	95.66454	710.1119	153.2446	332.9348	0.850105				
9	97.18071	494.7477	86.09419	239.1015	0.870532				
9	105.1566	450.0234	124.2753	239.3999	0.865028				
10	94.03737	725.2795	141.8892	333.9189	0.853199	89.4	±8.2	15	17
10	102.7316	537.9345	143.6547	276.3394	0.856968				
10	87.12724	526.013	146.6714	223.4038	0.83462				
10	83.88723	358.4952	28.60761	141.1664	0.84064				
10	80.15028	317.3455	55.63947	120.4249	0.830061				
14	92.79486	703.9958	67.37327	315.4321	0.860736	85.2	±4.2	6.4	7.50
14	83.95101	413.4325	59.77054	170.4435	0.866582				
14	82.66252	763.1294	172.2376	311.5823	0.85606				
14	86.62948	435.7494	71.71893	178.8589	0.832119				
14	80.53261	336.0777	48.74379	126.3706	0.824153				
18	78.58032	150.0283	40.96633	59.57151	0.8674	76.0	±7.4	1.7	2.2
18	73.69325	40.4532	13.03194	15.49946	0.883058				
19	74.7153	289.5867	22.11804	99.69039	0.826603	73.3	±6.8		9.3
19	75.17251	100.0072	22.32668	37.52445	0.866246				
19	70.30939	145.5559	22.91059	49.61998	0.854379				
20	75.38772	244.275	76.58532	91.75122	0.847664	84.2	±7.2	15	18
20	81.06873	434.1333	125.6954	171.6366	0.833568				
20	75.20905	298.6783	104.0468	111.1041	0.835172				
20	85.47001	309.043	70.94722	131.7096	0.86322				
20	93.46009	221.3544	70.18708	106.0667	0.869969				
20	95.37998	216.996	68.14307	106.0667	0.869981				

†U and Th concentrations are blank-corrected.
‡Ft denotes retained fraction of He after Farley et al. (1996).

TABLE 6. SUMMARY OF RADIOMETRIC AGES (IN Ma) AND EQUILIBRATION PRESSURES FROM PICKETT AND SALEEBY (1993)

Sample	Lithology	P (kb)	U/Pb (zircon)*	Sm/Nd (garnet)	U/Pb (titanite)	Ar/Ar (hornblende)	Ar/Ar (biotite)	Rb/Sr (biotite)	(U-Th)/He zircon
1	migmatitic hornblende gabbro	7.5	105 ± 1	96.8 ± 2.9	-	-	-	-	-
2	garnet biotite tonalite	9.4	101 ± 1	99.0 ± 3.1	-	-	-	-	-
3	migmatitic paragneiss	>7.6	~101	-	-	-	86.8 ± 0.3	87.4 ± 1.1	-
4	garnet biotite tonalite gneiss	-	112 ± 2	-	99 ± 2	-	-	87.5 ± 1.1	86.0 ± 2.5
5	migmatitic hornblende diorite	7.3	102 ± 1	95.9 ± 3.0	-	-	-	-	-
6	garnet hornblende tonalite gneiss	8.2	110 ± 2	-	-	91.4 ± 0.7	-	89.1 ± 1.2	
6b	amphibolitic gabbro layer	8.2	~110	102.2 ± 2.9	-	93.7 ± 1.6	-	-	-
7	hornblende biotite granodiorite gneiss	9.3	112 ± 2	-	102 ± 1	94.7 ± 0.7	85.1 ± 0.5	87.0 ± 1.1	-
8	biotite granite gneiss	-	112 ± 3	-	-	-	-	-	87.5 ± 3.5
9	epidote garnet tonalite gneiss	-	110 ± 2	-	-	-	-	89.2 ± 1.1	91.1 ± 7.7
10	granite gneiss	-	113 ± 2	-	-	-	-	-	89.4 ± 8.2
11	hornblende biotite tonalite	7.8	102 ± 1	-	-	-	88.0 ± 0.3	86.9 ± 1.3	-
12	hornblende biotite tonalite gneiss	8.8	111 ± 1	-	96 ± 2	93.8 ± 0.9	88.0 ± 0.3	84.1 ± 1.3	-
13	hypersthene biotite tonalite gneiss	-	115 ± 2	-	97 ± 1	-	-	86.6 ± 1.1	-
14	two pyroxene hornblende gabbro	-	102 ± 2	-	-	-	-	-	85.2 ± 4.2
15	migmatitic hornblende gabbro	4.2	~102	94.8 ± 2.7	-	-	-	-	-
16	biotite granodiorite gneiss	8.3	112 ± 1.5	-	95 ± 1	-	80.5 ± 0.3	84.0 ± 1.3	-
17a	hornblende biotite tonalite gneiss	8.0	110 ± 1	-	-	-	85.1 ± 0.5	86.5 ± 1.2	-
17b	hornblende diorite gneiss layer	-	~110	-	-	93.0 ± 0.6			-
17c	mylonite zone	-	~110	-	-	88.5 ± 1.2	81.4 ± 3.4	73.5 ± 1.0	-
18	two-pyroxene biotite hornblende tonalite gneiss	-	113 ± 2	-	-	-	-	84.2 ± 1.1	76.0 ± 7.4
19	Hypersthene biotite tonalite	-	101 ± 1	-	-	-	-	82.4 ± 1.0	73.3 ± 6.8
20	Biotite tonalite	-	100 ± 1.5	-	-	-	-	84.9 ± 1.5	84.2 ± 7.2
21	Hornblende biotite tonalite	6.9	99 ± 1	-	-	85.2 ± 0.4	81.6 ± 0.3	75.2 ± 1.1	

*U/Pb zircon ages from Saleeby et al. (1987), Pickett and Saleeby (1994), and GSA Supplementary Data Repository. Those ages shown as approximate, or as ranges are based on lithologic correlation to nearby dated localities.

zoic and Proterozoic zircon from the batholithic source regime. Most of the Bear Valley suite and pegmatite dikes yield concordant ages. A notable exception is the Bear Valley suite tonalite that is nested between the Tunis Creek gabbro and the arcuate migmatitic paragneiss body in the lower El Paso Creek area (Fig. 1). Field relations as well as zircon discordance patterns indicate assimilation of paragneiss and possibly orthogneiss by the Bear Valley suite tonalite in this locality. Small degrees of zircon inheritance or entrainment were also resolved in parts of the Tunis Creek gabbro. In general, however, most of the U/Pb zircon ages are apparently concordant, and such concordance is assumed to approximate igneous crystallization of the host rock. In our thermochronologic analysis, the U/Pb zircon ages for the orthogneisses and Bear Valley suite are mated with zircon saturation temperatures based on whole-rock trace element data to define an initial time-temperature (*t-T*) state for the complex. For the pegmatite dikes, U/Pb zircon ages are mated with water-saturated phase relations of trondhjemitic melts for their corresponding *t-T* datums.

The subset of orthogneiss zircon samples that were chosen for U/Pb titanite age determinations were selected based on their field settings traversing near- and far-field positions relative to crosscutting Bear Valley intrusives. Textural criteria were used as well. These criteria strived to select samples for which superimposed subsolidus plastic deformation was minimal, and for the recognition of a predominance of titanite grains that appeared to grow as an igneous phase in the original orthogneiss. The U/Pb titanite age data are presented in Table 2 along with the corresponding zircon ages for direct comparison. Low radiogenic lead contents and low uranium concentrations permit meaningful age determinations for only the $^{206}Pb/^{238}U$ systems. Titanite from samples 4 and 7 yield ages indicating complete, or nearly complete, resetting in the Pastoria Creek unit by Bear Valley suite magmatism. Samples 12, 13, and 16 from the Tejon Creek unit also show resetting, but with more prolonged high-temperature conditions pervading the sampled area. As discussed below, the prolonged high-temperature conditions in the eastern domain relative to the western domain is interpreted to reflect a higher volume of Bear Valley intrusives in the east as well as an eastward migration pattern in time with Bear Valley suite magmatism.

Sm/Nd Data

In Table 3, garnet Sm/Nd ages are reported on five samples for which there are thermobarometric data (Pickett and Saleeby, 1993). Three samples are from Bear Valley suite cumulate hornblende gabbros (1, 5, and 15). These are characterized by coarse metamorphic garnet growth (1–5 cm) superimposed over igneous textures. Textural relations indicate that garnet formation was at the expense of cumulate hornblende, and involved generally low degrees of partial melting with the production of trondhjemitic leucosomes. Samples 1 and 15 are incipiently migmatized, whereas the sample 5 site shows more extensive partial melt development. Sample 6b is an amphibolitic gabbro layer from tonalite gneiss of the Pastoria Creek unit. Garnet porphyroblasts up to 8 mm in diameter grew at the expense of hornblende in this sample, but partial melt development is not as clearly expressed as in the Bear Valley suite gabbro samples. Sample 2 is from an equigranular igneous-textured Bear Valley suite tonalite that intrudes both ortho- and paragneisses. Garnet in this sample is in apparent equilibrium with igneous phases and is thus considered igneous in origin.

Table 3 presents the Sm/Nd age data for garnet-matrix pairs. For the migmatitic gabbros, the leucosomes encasing the analyzed garnets were taken for the matrix $^{143}Nd/^{144}Nd$ and Sm/Nd determinations. Individual coarse garnet grains of 1.5–3 cm diameter were analyzed for each of the migmatitic gabbros, and such garnets poikiloblastically enclose leucosome material. Detailed petrographic studies indicate that many of the inclusion clusters are parts of anastomosing tubules of the encasing leucosomes that penetrate the garnet interiors. The inclusions were thus separated and analyzed as part of the leucosome matrices. For the sample 2 garnet tonalite, the 3–5 mm garnets were separated from the whole-rock matrix, and the residual matrix was run for the $^{143}Nd/^{144}Nd$ and Sm/Nd determinations. Inclusions were lacking or rare in such garnets. For the sample 6b amphibolitic gabbro, a cluster of 5–8 mm garnets was separated from the matrix. These garnets contained inclusions that resemble the partial melt inclusions from the migmatitic gabbros. They were likewise separated and run as part of the whole-rock matrix. The garnet-leucosome or whole-rock matrix Sm/Nd ages are between ca. 95 and 102 Ma. The spread in these ages is outside the analytical uncertainties of the individual age determinations and is considered geologically significant. In particular, the migmatitic gabbros yield the youngest ages, which is a point that will be discussed in more detail below.

Closure temperatures for Sm/Nd garnet systems in high-grade crustal terranes have been suggested to be as high as ~900 °C and as low as ~600 °C (Cohen et al., 1988; Mezger et al., 1992). It has been further suggested that major cations involved in the exchanges for which garnet-based thermobarometric systems hinge share similar diffusivities as Sm and Nd (Elphick et al., 1985; Ganguly et al., 1998). Following these studies, we have chosen to use the thermobarometrically determined temperature values for each sample analyzed as a principal constraint for the respective Sm/Nd closure temperatures in our thermochronologic analysis. These temperatures lie in the range of ~600 to ~750 °C. We also relate the coupled pressure determinations to the respective Sm/Nd ages in estimating the barochronometric history of the complex for the high-temperature part of its *P-T* history. As suggested by Mezger et al. (1992), garnet closure in high-grade terranes, such as the Tehachapi complex, reflects conditions traversed during the retrograde part of the respective *P-T* path. This view is in general supported in our pressure-temperature-time analysis of the Tehachapi complex.

Rb/Sr Data

Biotite/whole-rock Rb/Sr ages are reported for a number of Bear Valley Springs intrusives and orthogneisses, and for one migmatitic paragneiss sample. These data are presented along with the

coupled Ar/Ar data in Table 4. A number of the biotite Rb/Sr samples had whole-rock Rb/Sr data reported in Saleeby et al. (1987). For these samples, biotite separates were taken from splits of the whole-rock fractions analyzed, and the published whole-rock data were used for the age calculations. For the remainder of the samples, new whole-rock data are reported along with the biotite mineral data. Biotite/whole-rock isochron ages were calculated after Ludwig (1999). Such ages for the chief domains of the complex lie between 89 and 84 Ma. Samples along the basal domain are as young as ca. 73 Ma, and the Bear Valley Springs pluton sample from the northern end of the study area yields a ca. 75 Ma age. Rb/Sr mineral data are also presented for several of the hornblende separates. Most of these yielded too low Rb/Sr ratios to solve for mineral/whole-rock isochrons. The one exception is sample 21 from the Bear Valley Springs pluton, which yielded a ca. 88 Ma age. This is ~4 m.y. older than the corresponding Ar/Ar age.

Study of Table 4 reveals that in general the biotite Rb/Sr ages were set prior to the biotite Ar/Ar ages, as expected from the difference in preferred closure temperatures (Table 1). Some of the coupled samples show concordance between the two different systems within analytical uncertainty. For the sample 17c mylonite, sample 12 tonalite gneiss, and sample 21 from the Bear Valley Springs pluton, the biotite Rb/Sr ages are significantly younger than the coupled Ar/Ar ages. This raises the possibility of subsolidus alteration of the whole-rock Rb/Sr systematics, which would induce geologic errors in the biotite ages that are not reflected in the analytical uncertainties. Such a concern is amplified by the fact that coupled $\delta^{18}O$ whole-rock/zircon measurements in the complex typically yield +3‰ shifts for the whole-rock values, indicating substantial subsolidus exchange of oxygen in the whole-rock systems (Saleeby et al., 1987; Lackey et al., 2005). Regardless of this possible complication, a whole-rock isochron of 116 ± 5 Ma was determined for a large set of orthogneiss samples (Saleeby et al., 1987), and the new orthogneiss whole-rock data presented here plot in general along this isochron. The interpretation of this isochron as an igneous age approximation for the orthogneisses is in agreement with the U/Pb zircon data, and thus major subsolidus alteration of the Rb/Sr systematics in the orthogneisses was not intense nor pervasive enough to upset the isochron systematics. The whole-rock values for samples 12 and 17c plot significantly off this isochron, suggesting a localized chemical alteration effect in distorting the calculated age. The Bear Valley suite does not define a coherent isochron, but nevertheless sample 21 plots as a clear outlier point in relation to the rest of the Bear Valley suite data cluster. These possible chemical alteration effects are used as a basis to exclude the sample 12, 17c, and 21 data from our thermochronological analysis.

Ar/Ar Data

Ar/Ar age data for biotite and hornblende are presented along with the Rb/Sr biotite data in Table 4. Sample selection for the Ar/Ar work focused on samples for which thermobarometric data were published in Pickett and Saleeby (1993). Such sample selection was not only motivated by direct linking of the thermobarometric and Ar/Ar data, but also of necessity in selecting samples for which subsolidus textural modification of both hornblende and biotite was minimal. Table 4 presents $^{40}Ar/^{36}Ar$-$^{39}Ar/^{36}Ar$ isochron, $^{40}Ar/^{39}Ar$ total fusion, and $^{40}Ar/^{39}Ar$ plateau ages. In general, these ages are within analytical uncertainty of one another. In our thermochronologic analysis below, we cite plateau ages. One notable exception is the sample 17c mylonite biotite separate, which did not yield a plateau, so its total fusion age, which is in agreement with its isochron age, is cited. Plateau definition is based on Ludwig (2001). Ar/Ar incremental heating and isochron plots are provided for each sample in the GSA Data Repository.

The biotite Ar/Ar ages for the chief domains of the complex show similar scatter (ca. 88–81 Ma) as the biotite Rb/Sr ages (ca. 89–84 Ma), but offset to the young side. This is suggested to generally reflect the difference in preferred closure temperatures between the two isotopic systems in biotite (Table 1), although structural and chemical alteration factors, as discussed below, are considered as well. One sample in particular (number 16) is suspect in this regard. Its Rb/Sr and Ar/Ar ages are both distinctly younger than biotite Rb/Sr and Ar/Ar ages from the chief domains, and they strongly resemble ages from the basal domain. Based on structural arguments presented below, the sample 16 biotite data are treated as basal domain. Coupled with the exclusion of the sample 12 Rb/Sr age discussed above, the biotite data clusters tighten for the chief domains at ca. 88–85 Ma for Ar/Ar and ca. 89–86 Ma for Rb/Sr. The hornblende Ar/Ar ages for the chief domains cluster at 91–95 Ma. The sample 17c mylonite yields younger biotite and hornblende Ar/Ar ages at ca. 81 Ma and ca. 89 Ma, respectively. As discussed below, these younger ages as compared to those of the chief domains are considered to have undergone reheating in conjunction with the emplacement of the underlying schist. Sample 21 from the Bear Valley Springs pluton at the northeast corner of the study area also yields relatively young biotite and hornblende Ar/Ar ages of ca. 82 Ma and ca. 85 Ma respectively. As discussed below, these younger ages are suggested to represent a combination of a slightly different exhumation history in the northeast region as well as the regional across-strike age and related subsolidus thermal gradient in the Sierra Nevada batholith.

(U-Th)/He Zircon Data

(U-Th)/He zircon data are presented in Table 5 for a number of samples that have also had U/Pb zircon and Rb/Sr biotite ages determined. Additional supporting data for these samples are given in the GSA Data Repository. The ages reported and used in our analysis are averages of two to seven single-crystal determinations. As is commonly observed, the single-crystal age determinations for each sample scatter more than the analytical uncertainties for the given analyses, and thus the uncertainties cited in Table 5 represent primarily intrasample age heterogeneities. This grain-to-grain variability most likely arises from spatial heterogeneity in U and Th concentrations affecting both the α ejection correction and the effective closure temperature.

The He-zircon ages for the chief domains of the complex lie in the range of ca. 91–85 Ma. Those samples which fall at the high end of this array yield the highest uncertainties. This is significant for our thermochronologic analysis because the two highest ages of ca. 90 Ma and ca. 91 Ma are slightly older than the oldest biotite Ar/Ar and Rb/Sr ages, which were presumably set at ~100 °C higher temperatures than the He-zircon systems. Pertinent to this subject is the uncertainty on the cooling rate for the complex and the uncertainty that it casts on our preferred closure temperature range for the He-zircon system (Table 1). The 170–190 °C range cited from Reiners et al. (2004) is based on a canonical cooling rate of 10 °C/m.y., although in the analysis offered below we prefer a much faster cooling rate in the 100s °C/m.y. range. Such a rapid cooling rate could raise the effective closure temperature range by 30–40 °C (Dodson, 1973), which would push the upper limit of the He-zircon range to within 10–20 °C of the lower limit for Ar/Ar biotite. Textural modification of biotite by plastic deformation, as discussed above, and a lack of such for zircon, could also be a factor in effectively converging the limits of their respective closure temperature fields.

Two He-zircon ages were determined for samples from the basal domain (samples 17 and 19). These yield significantly younger ages (ca. 76 Ma and ca. 73 Ma) than the samples from the chief domains of the complex. These younger ages are interpreted below to carry important information on the tectonic underplating of the Rand Schist. Sample 20 is from the Bear Valley Springs pluton as exposed in the northeast corner of the study area. It yields a He-zircon age of ca. 84 Ma. This sample offers an important datum in our regional analysis in that it is from the lowest-pressure sample of the entire study area (6.9 kbar), and lies within the midst of the well-defined segment of the regional north-south pressure gradient in the Sierra Nevada batholith.

The He-zircon data of the western domain are complemented by zircon and apatite fission track and (U-Th)/He apatite data from the Pastoria Creek unit in the lower Grapevine Canyon area (Naeser et al., 1990; Niemi et al., 2004). The zircon and apatite fission track ages are 80.8 ± 11.5 Ma and 70.5 ± 12.9 Ma, respectively, and the He-apatite age is 59 ± 5 Ma. The zircon fission track data overlap considerably with the He-zircon data and thus do not provide any additional constraints. The apatite data are used in conjunction with the stratigraphic constraints of middle Eocene nonconformable overlap to constrain the low-temperature cooling history of the complex.

THERMOCHRONOLOGY OF THE TEHACHAPI COMPLEX

Initial State

The thermal evolution of the Tehachapi complex follows a retrogressive *P-T* path that descended from widely established tonalite and wet basalt solidus conditions culminating at ca. 100 Ma. We begin our treatment of the thermochronometry of the complex with a discussion of the initial high-temperature batholithic environment. The tremendous volume of juvenile batholithic crust that constitutes the Sierra Nevada batholith is born out by the fact that the oblique crustal section exposes primarily batholithic rocks from subvolcanic to ~10 kbar levels. This is shown to also characterize the region beneath the expansive shallower-level exposures of the Sierra Nevada batholith to the north by seismic data that yield velocities typical of felsic batholithic rocks extending from surface levels down to the Moho at ~30–40 km depths (Ruppert et al., 1998; Fliedner et al., 2000). These relations, in conjunction with regional geochronologic and isotopic data, indicate that virtually the entire crust was reconstituted rapidly under arc magmatic conditions (Ducea, 2001; Saleeby et al., 2003). In the case of the Bear Valley Springs pluton and its coeval overlying suite of volcanic-hypabyssal rocks, an entire ~30 km thick section of juvenile arc crust underlying an area of at least 30 km in width by ~100 km in length was generated in as little as ~5 m.y. (Saleeby and Busby-Spera, 1986; Saleeby et al., 1987). Such high magma flux and pluton accumulation rates appear to be typical of much or all of the Sierra Nevada batholith (Coleman and Glazner, 1998; Ducea, 2001). In such an environment, we must ask at what temporal and spatial scales newly formed lower crust descends through its solidus. In the case of the Tehachapi complex, U/Pb titanite ages of 102–95 Ma that are widely dispersed in the orthogneisses (Table 2) indicate prolonged high-temperature conditions for the gneisses, and/or their extensive reheating by Bear Valley suite magmatism. Textural and field relations indicating widespread garnet formation in conjunction with low degrees of partial melting in Bear Valley suite mafic cumulates in conjunction with Sm/Nd garnet ages as young as ca. 95 Ma for such garnets further indicate prolonged near-solidus conditions persisting for up to ~5 m.y. following Bear Valley suite magmatism.

In the discussions that follow, we first treat the time-temperature paths of the western and eastern domains of the complex from high- to low-temperature conditions. The culmination of Bear Valley suite magmatism is for the most part treated as the initiation of these time-temperature paths. Inspection of the Table 6 compilation of isotopic ages reveals that regardless of sharing the same initiation, the Bear Valley Springs pluton samples followed a very different time-temperature path through medial- to low-temperature conditions than the western and eastern domains. These differences are treated in the context of the temporal patterns in the migration of Sierra Nevada batholith magmatism, and spatial patterns in depth of exposure. The thermochronometry of the basal domain is treated later in the context of the decompression and exhumation history of the complex, and the tectonic underplating of the Rand Schist. A crustal-scale conductive cooling model has been generated for the Sierra Nevada batholith that is based on the ~3 mm/yr regional eastward migration rate of magmatism, and also incorporates incremental injection of magma pulses that are of appropriate scale for application to the Tehachapi complex (Barton and Hanson, 1989). This model does not account for exhumation during composite batholith growth, although a number of aspects of this model are used as a reference in our analysis below.

Western Domain

Figure 2A is a time-temperature (*t-T*) plot for the western domain data. All data points for this domain are shown on the plot. The garnet and titanite points labeled 4, 6b, and 7 are shown with their analytical uncertainties and temperature range bars and are treated separately from the main data array. The main data points are shown with shaded areas that define high-confidence fields based on closure temperature ranges (Table 1) and the error-weighted means of the respective age determinations. Also shown on Figure 2 are apatite fission track and (U-Th)/He ages from the lower Grapevine Canyon area (Naeser et al., 1990; Niemi et al., 2004). The high-temperature end of the main array is constrained by the Sm/Nd garnet ages for the Bear Valley intrusives, which nearly converge with the Bear Valley suite U/Pb zircon ages. The temperatures used for the garnet data points are the thermobarometrically determined values. The U/Pb zircon ages for western domain pegmatite dikes lie within the Bear Valley suite garnet cluster. One of the pegmatite samples (5b) is intergradational with nonpegmatitic leucosome material of the sample 5 migmatitic diorite. Its U/Pb zircon age is nearly indistinguishable from the corresponding Sm/Nd garnet age. The main data array generally lies along a linear trend shown by the dashed line corresponding to a cooling rate of ~40 °C/m.y. This regression is constrained to commence with the youngest Bear Valley suite U/Pb zircon age determined in the western domain. This is not our preferred cooling trajectory for the western domain. The preferred trajectory is discussed below in the context of other factors, and includes the low-temperature apatite data.

We turn now to the sample 4, 6b, and 7 data points. Exposures in the western domain are dominated by the quartzofeldspathic gneiss of Pastoria Creek (Fig. 1). Both east and west of the Pastoria Creek area, gabbroic to tonalitic intrusives of the Bear Valley suite are abundant. In the Grapevine Canyon area, gabbroic to tonalitic intrusives of the younger suite and migmatitic paragneisses dominate the exposures. Regardless of the

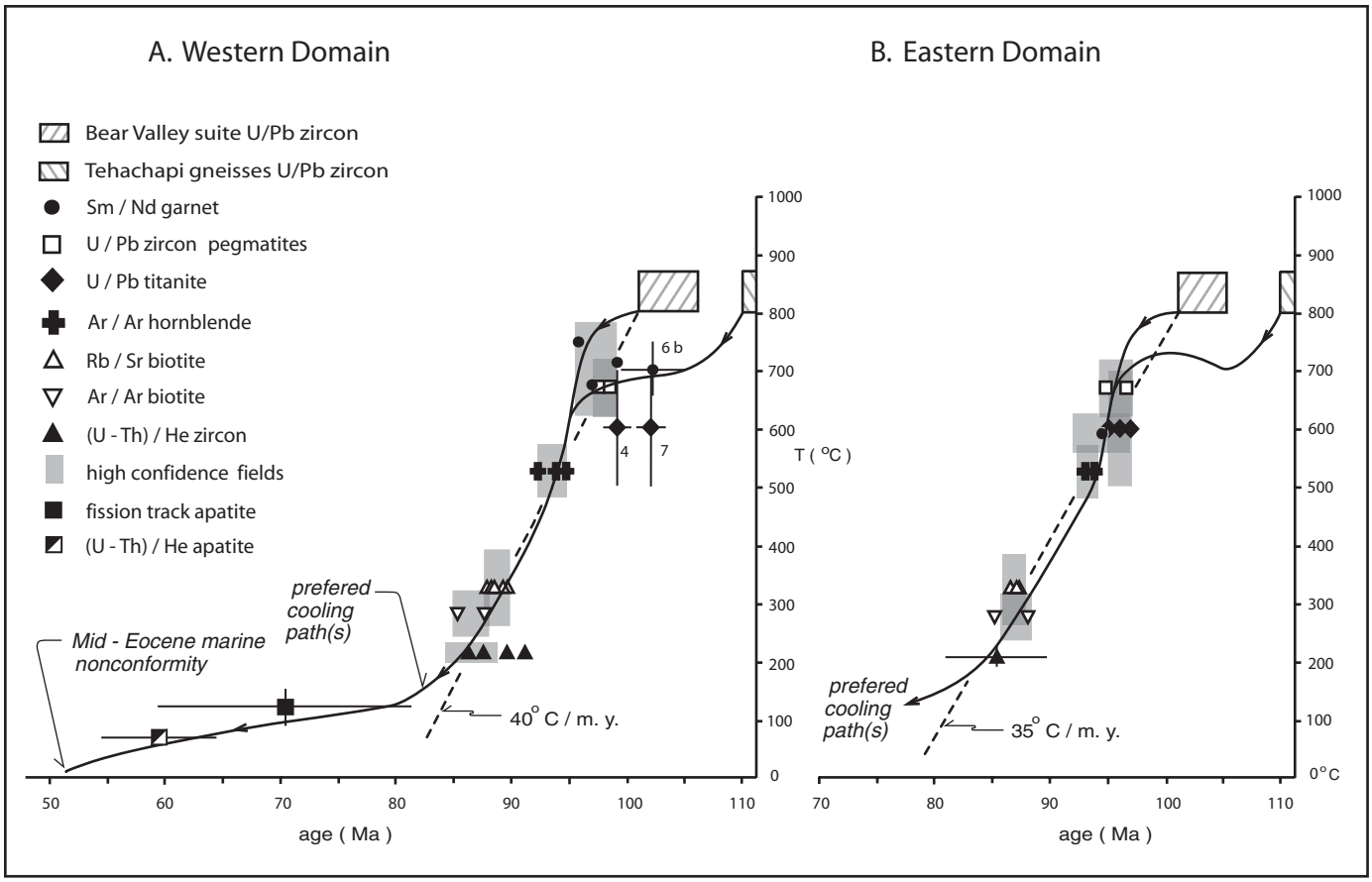

Figure 2. Time-temperature (*t-T*) plots for thermochronometric data from western domain (A) and eastern domain (B) of Tehachapi complex. Shaded areas represent high-confidence fields based on closure temperature ranges from Table 1, and from error-weighted means of multiple analyses of a given isotopic system (data tabulated in GSA Data Repository), or for individual analyses 2σ uncertainty used. U/Pb zircon ages from Saleeby et al. (1987), Pickett and Saleeby (1994), and GSA Data Repository. Samples not labeled in A: garnet Sm/Nd (1, 2, 5), hornblende Ar/Ar (6, 6b, 7), biotite Rb/Sr (3, 4, 6, 7, 9) and Ar/Ar (3, 7), He-zircon (4, 8, 9, 10). Apatite fission track and He data after Naeser et al. (1990) and Niemi et al. (2004), respectively. Samples in B: garnet Sm/Nd (15), titanite U/Pb (12, 13, 16), hornblende Ar/Ar (12, 17b), biotite Rb/Sr (11, 13, 17a) and Ar/Ar (11, 12, 17a), and He-zircon (14). Cooling paths discussed in text.

inhomogeneous distribution of Bear Valley intrusives through the gneisses, U/Pb titanite ages on widely spaced gneiss samples 4 and 7, and the Sm/Nd garnet age of sample 6b, indicate near-pervasive reheating of the gneisses to as high as ~700 °C during intrusion of the Bear Valley suite. Inspection of Figure 1 reveals that samples 6b and 7 lie in the far field relative to significant Bear Valley suite pluton emplacement, while sample 4 is more proximal to Bear Valley suite tonalite bodies. The ~3 m.y. offset in age between sample 4 and samples 6b and 7 is interpreted to reflect a thermal gradient within the Pastoria Creek unit related to Bear Valley suite magmatism. This gradient is further interpreted to have affected primarily the high-temperature chronometers, having dissipated by hornblende Ar/Ar closure temperatures. Accordingly, the western domain is considered to have initiated its cooling history with significant variation in its initial state. We will return to this below in the context of other data constraints and the thermal modeling of Barton and Hanson (1989).

Eastern Domain

Figure 2B is a time-temperature plot for the eastern domain thermochronometric data. Samples 17c, 18, and 19 as well as the sample 16 biotite data are omitted from the plot and treated below as basal domain data on the basis of both textural relations and structural position. The format of Figure 2B is the same as for Figure 2A. High-confidence fields are defined on the basis of closure temperature ranges (Table 1) and the error-weighted means of ages from multiple samples, or the 2σ uncertainties for individual age determinations (i.e., garnet and He-zircon). Exposures in the eastern domain consist of subequal gneisses and Bear Valley intrusives. The orthogneisses consist of the eastern bodies of the Pastoria Creek unit and the tonalite gneiss of Tejon Creek. These are extensively intruded by gabbroic cumulates and tonalites of the Bear Valley suite. The eastern domain is bounded to the east by the basal zone of the Bear Valley Springs pluton. Here the Tejon Creek tonalite gneiss and screens of granulite-grade paragneiss dip northeast under the pluton. Southward the gneisses are cut out by the Bison Peak hypersthene tonalite of the Bear Valley suite (Fig. 1). Thus, for the most part, the orthogneisses of the eastern domain appear to be enclaves within the Bear Valley suite. U/Pb titanite ages from widely spaced orthogneiss samples of the eastern domain indicate extensive reheating and prolonged high-temperature conditions related to Bear Valley suite intrusive activity. Comparison of the titanite data points of Figure 2B with those of Figure 2A shows that unlike the western domain, the eastern domain titanite ages lie within the main data array.

The high-temperature end of the eastern domain array is defined by the clustering U/Pb pegmatite and orthogneiss titanite data, and by the sample 15 Sm/Nd garnet age. The medial to lower temperature ranges as defined by the hornblende, biotite, and He-zircon data are nearly indistinguishable from those of the western domain. The eastern domain data define a linear array similar to that of the western domain, but with a slightly slower apparent cooling rate of ~35 °C/m.y. The eastern and western domains share similar overall cooling histories, except for longer-lasting and perhaps more pervasive initial high-temperature conditions in the eastern domain related to a higher concentration of Bear Valley intrusives. There are no low-temperature (<200 °C) data available for the eastern domain. As with the western domain, the preferred cooling path of the eastern domain is discussed below.

Basal Zone of Bear Valley Springs Pluton

The southwest margin of the Bear Valley Springs pluton is interpreted as its basal zone on the basis of (1) the continuous southward deepening of the pluton shown primarily by Al-in-hornblende barometry (Ague and Brimhall, 1988; Pickett and Saleeby, 1993), (2) the attitudes of magmatic and solid-state foliations indicating that the gneisses dip concordantly beneath the pluton (Fig. 1), and (3) the high concentration of Bear Valley intrusives within the eastern domain. The last point requires more attention. The Bear Valley suite in the eastern domain is dominated by pyroxene tonalites, which are also common in the deeper levels of the Bear Valley Springs pluton. Also, hornblende-rich cumulates such as the Tunis Creek gabbro body occur in the Bear Valley Springs pluton, but in lower proportions relative to tonalites and gabbros of the eastern domain. It is postulated that the Bear Valley intrusives in the eastern domain, prior to the deep exhumation of the complex, once coalesced upward into virtual continuity with the Bear Valley Springs pluton above much or all of the eastern domain gneisses. The contrasts in the high-temperature histories between the western and eastern domains reflect the more proximal position of the eastern domain within the principal zone of Bear Valley suite magmatism.

Figure 3 is a plot that relates the thermochronometric data to the regional time-space migration patterns in high-volume magmatism of the Sierra Nevada batholith. Samples treated as part of the basal domain, and biotite Rb/Sr ages considered as suspect in terms of possible whole-rock system alterations, are omitted from the plot. The relative positions of the data points were corrected for post–Sierra Nevada batholith 45° clockwise rotation (after Kanter and McWilliams, 1982) and then projected onto an ~N60°E section line, which approximates the across-strike trace of the greater Sierra Nevada batholith. The data points include U/Pb zircon ages for the orthogneisses, Bear Valley suite and pegmatite dikes, and the thermochronometric data. The approximate positions of the 6, 7, 8 and 9 kbar igneous pressure isopleths based on the most robust thermobarometric determinations for the principal solidus conditions of the complex are plotted as well. The U/Pb zircon ages that are shown at the eastern margin of the plot at pressures of <6.9 kbar are projected from Figure 2 of Saleeby et al. (1987) as a means of better elucidating the regional time-space patterns in plutonism for the study area.

The spatial variations in ages for the higher-temperature chronometers in general follow the eastward migration pattern in regional Sierra Nevada batholith magmatism shown on Figure 3 at ~3 mm/yr (after Chen and Moore, 1982). The U/Pb zircon ages for the orthogneisses and Bear Valley suite generally follow this

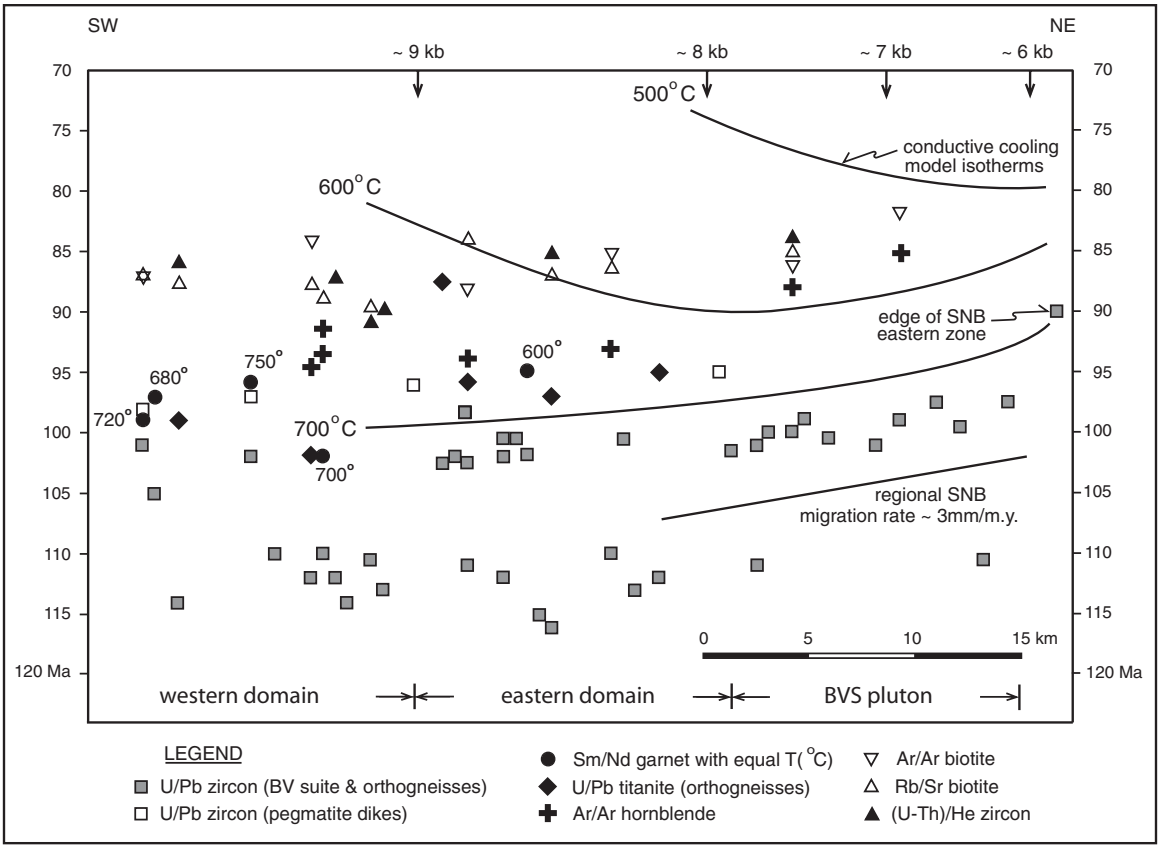

Figure 3. Projection of thermochronometric data (Table 6) and U/Pb zircon data (Saleeby et al., 1987; Pickett and Saleeby, 1994; GSA Data Repository) onto regional cross-sectional trace of Sierra Nevada batholith (SNB) as means of displaying spatial patterns in magmatism and cooling. Samples interpreted as having been reheated in conjunction with Rand Schist underplating are omitted (sample 16 biotite Rb/Sr and Ar/Ar, and samples 17c, 18, and 19). Regional pluton migration rate of ~3 mm/yr after Chen and Moore (1982). Approximate positions of igneous pressure isopleths shown across top of figure. Equilibrium temperatures of garnet points after Pickett and Saleeby (1993). Crustal-scale conductive cooling model for SNB (after Barton and Hanson, 1989) mapped as 700 °C, 600 °C, and 500 °C isotherms onto time-distance-pressure space demonstrates temporal and spatial relations of divergence of data from simple crustal-scale cooling without exhumation. BVS—Bear Valley Springs.

rate, but as is common for the southwestern Cordilleran batholithic belt, the Early Cretaceous western zone shows much more scatter in ages than the Late Cretaceous eastern zone (Saleeby and Sharp, 1980; Silver et al., 1979; Stern et al., 1981; Chen and Moore, 1982; Clemens-Knott and Saleeby, 1999). The high-temperature thermochronometric systems of U/Pb titanite and Sm/Nd garnet, as well as the U/Pb zircon ages for the pegmatite dikes, were all set spatially with time in an eastward migration rate that approximates the plutonism rate. The Ar/Ar hornblende, biotite Ar/Ar and Rb/Sr, and the (U-Th)/He zircon ages do not yield a spatial migration pattern across the western and eastern domains. Traversing eastward from the Bear Valley Springs pluton–gneiss complex contact zone, a possible spatial variation pattern in cooling for the hornblende and biotite ages is suggested by the data. Note that supplemental hornblende and biotite K/Ar ages from Ross (1983) for the Bear Valley Springs pluton, which were determined close to the sample 20 site, were added to Figure 3.

The inflections in the spatial variation patterns of the biotite and hornblende arrays between the chief domains and the Bear Valley Springs pluton could signal a change from predominately tectonic controls on cooling in the west to more ambient regional batholithic cooling patterns in the east related to the eastward migration of magmatism. Samples 20 and 21 from the Bear Valley Springs pluton show large discordances between U/Pb zircon and Ar/Ar hornblende and biotite ages: ~12 m.y. and ~16 m.y. for hornblende, and ~14 m.y. and ~19 m.y. for biotite, respectively. These far exceed the average discordance values for the greater Sierra Nevada batholith of ~2 m.y. for hornblende and ~6 m.y. for biotite (Barton et al., 1988), and undoubtedly reflect the much deeper level of emplacement and subsequent exposure of the southern part of the Bear Valley Springs pluton as compared to the rest of the Sierra Nevada batholith to the north.

The conductive cooling model for the Sierra Nevada batholith of Barton and Hanson (1989) suggests that at ~25–30 km

depths hornblende Ar/Ar systems could lag ~20 m.y. behind igneous emplacement ages, and that biotite Ar/Ar and Rb/Sr and He-zircon systems remain open indefinitely. In order to view the implications of this model in the context of our data, the 500 °C, 600 °C, and 700 °C isotherms of the model have been mapped onto the time-distance-pressure space of Figure 3. These isotherms are mapped principally for the eastern and Bear Valley Springs domains because the coherency of the pluton migration pattern breaks down in the western domain. The high-temperature cooling history of the complex in comparison to the theoretical 700 °C isotherm is discussed below. Of interest here are the 600 °C and 500 °C isotherms, which bracket the hornblende Ar/Ar closure temperature. Inspection of these isotherms show that hornblende Ar/Ar closures were ~15–20 m.y. early in the eastern and adjacent part of the western domains, relative to the model. Traversing eastward into the Bear Valley Springs pluton, the hornblende closure times rapidly approach that predicted by the model. Inspection of the 500 °C isotherm demonstrates the point made above of the biotite Ar/Ar and Rb/Sr and the He-zircon systems potentially remaining open indefinitely. These relations suggest that exhumation was a first-order process in controlling the cooling history of the western and eastern domains, and was less so in the Bear Valley Springs pluton where ambient cooling patterns of the batholith appear to have had a greater influence.

Inspection of the 700 °C isotherm suggests that near-solidus conditions can persist for up to ~5 m.y. at ~30 km depths in the wake of the migrating pluton emplacement pattern. For the western domain, there is reasonable correlation of the 700 °C isotherm with the thermobarometrically determined garnet temperatures, which are also shown on the plot. The divergence of the eastern domain lower-temperature and younger garnet data point from the model mimics the hornblende pattern, and again suggests that exhumation may have been instrumental in its cooling history. We turn now to the subject of exhumation.

DECOMPRESSION, COOLING, AND EXHUMATION OF THE TEHACHAPI COMPLEX

In this section, we focus on the decompression and early exhumation history of the Tehachapi complex. Thermobarometric and chronometric data as well as select petrogenetic relations are leveraged against one another in the derivation of a cooling and decompression history, and these with other considerations are in turn used to constrain the exhumation history.

Decompression

Garnet-based thermobarometric and Al-in-hornblende determinations of equilibration pressures cluster at ~8–10 kbar for much of the Tehachapi complex (Pickett and Saleeby, 1993). However, some important discrepancies arose in this work, all of which were for samples that underwent low degrees of partial melting at the culmination of Bear Valley suite magmatism. This includes the Bear Valley suite migmatitic gabbroid samples 1, 5, and 15, which yielded pressures of 7.5, 7.3, and 4.2 kbar respectively. Each of these samples lies adjacent to tonalitic rocks that yield pressures in the ~8–9 kbar range. Sample 15 also lies adjacent to migmatitic paragneiss that yields a pressure of 4.3 kbar as well as other migmatitic gabbro samples that yielded pressures of ~4 kbar. The aberrant lower pressure determinations are considered to carry important pressure-temperature-time information when interpreted in the context of the thermochronometric data and petrogenetic relations.

Figure 4 is a pressure-time plot for samples that have both garnet thermobarometric and Sm/Nd age data. The lower three points consist of Bear Valley suite migmatitic gabbros. The highest-pressure point is the sample 2 Bear Valley suite tonalite, and the data point with the oldest Sm/Nd age is the sample 6b amphibolitic gabbro layer from the Pastoria Creek gneiss unit. The uncertainties in the data points are large in comparison with the data spread, but nevertheless an overall trend of decompression with time is apparent. A linear regression through the array yields a decompression rate of ~0.65 kbar/m.y. Alternatively, a more complex curvilinear path encompassing a modest increase in pressure between ca. 102 Ma and ca. 99 Ma followed by a more rapid decompression rate of ~2 kbar/m.y. may be fit more precisely through the data. Petrogenetic relations of garnet formation during partial melting of the migmatitic gabbros in conjunction with garnet zonation patterns discussed below, and a closer assessment of the thermochronometric data, lead us to favor the second nonlinear path.

Cooling and Decompression

An apparent cooling rate for the Tehachapi complex of ~35–40 °C/m.y. can be derived from the Figure 2 arrays. This assumes a linear cooling rate, which in the analysis below is not favored. Steep garnet rim zonation patterns that are exhibited in all garnets analyzed for thermobarometry suggest that at the times of garnet closure, cooling rates may have been as high as ~500 °C/m.y. (Pickett, 1991; Spear, 1991; Pickett and Saleeby, 1993). Examination of Figure 2 reveals that a much more rapid cooling rate, conceivably in the 100s °C/m.y. range, can be fit through the high-temperature-range garnet and the medial-range hornblende fields. Such a steep cooling curve cannot be extended through the lower-temperature fields, which in effect requires a deceleration in cooling between the hornblende and biotite fields. A rapidly accelerating and then decelerating cooling trajectory is accordingly shown for our preferred cooling paths on Figure 2. This honors the garnet rim zonation data, and also explains why the garnet and titanite age data correlate reasonably well with the conductive cooling model while the hornblende age data diverge sharply (Fig. 3).

Preferred cooling paths shown on Figure 2 commence with their solidus to hot subsolidus trajectories derived from the Barton and Hanson (1989) model. These initial paths are deflected into cooling trajectories that honor the thermochronometric data. In the case of the western domain gneisses, a thermal recharge from

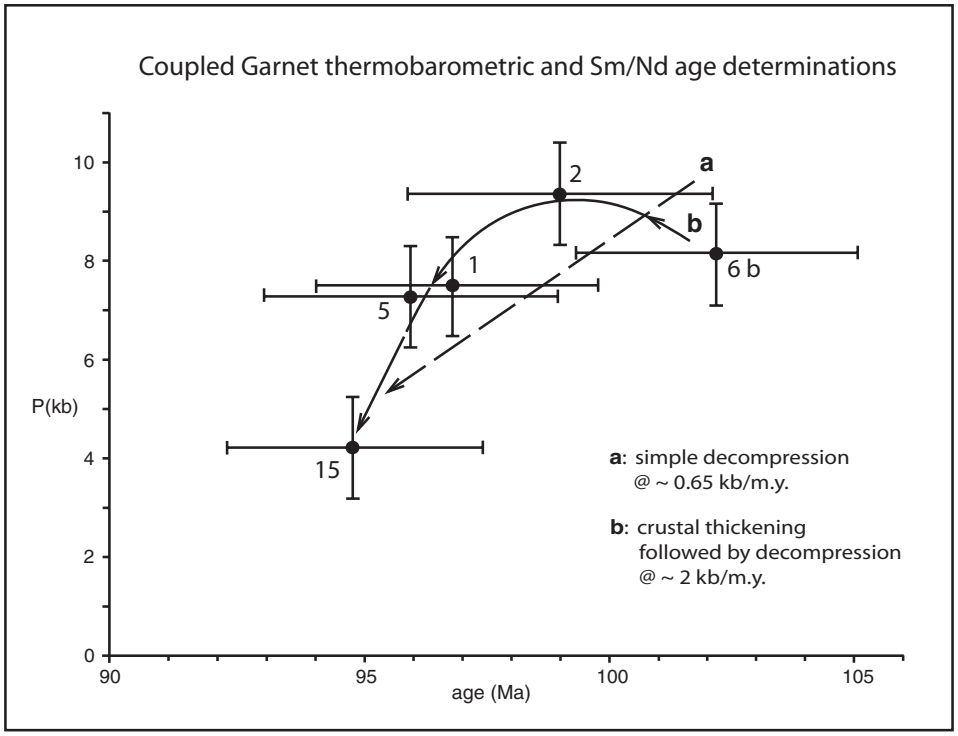

Figure 4. Plot of coupled garnet thermobarometric and Sm/Nd ages (Pickett and Saleeby, 1993) (Table 3). Two possible decompression paths are shown: simple linear trend with time (a); and preferred path (b) with modest increase followed by rapid decrease in pressure.

Bear Valley suite magmatism flattens the trajectory at ~700 °C, facilitating a path through the titanite and 6b garnet points. A more intense thermal recharge is required for the eastern domain in order to accommodate the titanite data, and is further indicated by the map-scale relations discussed above. The subsolidus segments of the Bear Valley suite curves diverge sharply from the simple conduction model at ca. 97 Ma, following a path through the garnet to hornblende segment of the trajectory. The resulting inflection in the cooling path is interpreted as a tectonic signal implying a profound event commencing at ca. 97–95 Ma. This inflection coincides in time with the inflection in the preferred barochronometric curve derived from the garnet data (Fig. 4). Accordingly, rapid cooling and rapid decompression are considered to signal the same tectonic event.

Garnet is a key phase in the pressure-temperature-time analysis of the complex. Widespread garnet growth characterizes the gneisses as well as much of the Bear Valley suite (Ross, 1989; Pickett and Saleeby, 1993). The garnets occur in several settings yet have remarkably consistent compositions and zonation patterns typified by compositionally flat interiors and steeply zoned rims (type "c" of Selverstone and Chamberlain, 1990). Such compositional profiles are interpreted to represent prolonged high-temperature conditions followed by rapid cooling. These compositional patterns are present in grain sizes that span millimeter to at least 5 cm scales. In metaigneous protoliths, the garnets occur in two main textural settings. (1) In hornblende-poor, biotite-bearing tonalites and granodiorites, they occur at millimeter scales in apparent equilibrium with igneous phases. In a number of these tonalites, euhedral epidote is embayed into biotite in a fashion also suggestive of igneous growth under high-pressure conditions (Sams and Saleeby, 1988; Zen, 1989). (2) In hornblende-rich tonalite, diorite, and gabbro, garnet occurs as a "subsolidus" phase commonly superimposed over primary igneous features, and locally over high-temperature deformation fabrics. Such garnets occur as scattered porphyroblasts and poikiloblasts commonly up to 2–3 cm and locally up to 10 cm in diameter, and also as fine-grained concentrations along fractures. In this setting, garnet formed at the expense of hornblende, which also resulted in the production of quartz and plagioclase. In numerous locations, the quartz-plagioclase products represent trondhjemitic leucosomes in mafic migmatite (Fig. 5). Such migmatization is locally observed in amphibolitic gabbro-diorite layers of the gneisses and is common in hornblende-rich cumulates of the Bear Valley suite. The degree to which discernable trondhjemitic leucosome and garnet melanosome have formed is roughly correlative to the hornblende modes of the protolith. Some of the larger leucosomes contain pegmatitic lenses or domains (Fig. 5C), which resemble meter-scale pegmatite dikes that are volumetrically insignificant but widespread in the complex. Inspection of Figure 2 and Table 6 shows that U/Pb zircon ages on the pegmatite dikes generally coincide with the Sm/Nd garnet ages on the Bear Valley suite migmatitic gabbros. These relations suggest

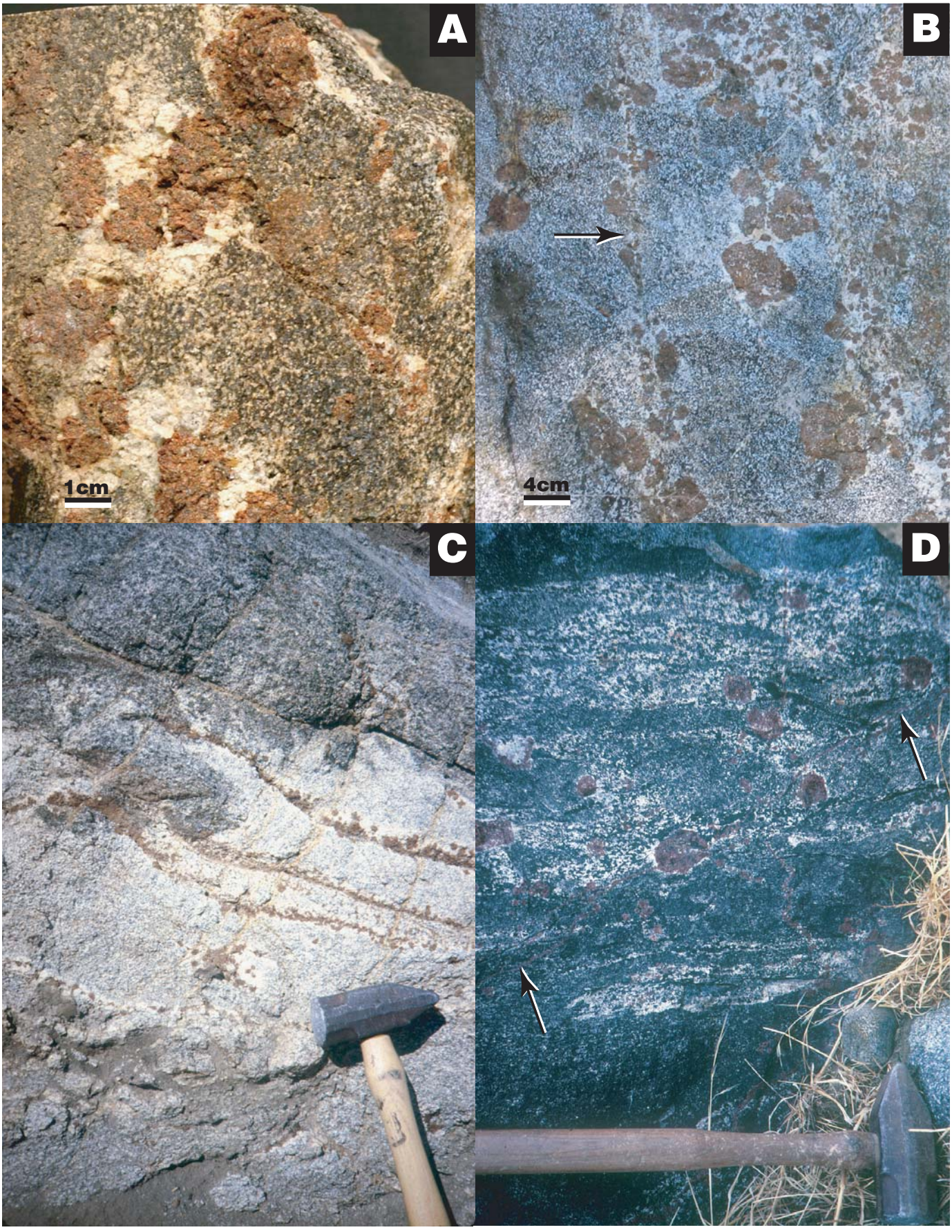
A
1cm
B
4cm
C
D

that localized migmatization of the complex occurred in association with pegmatite dike generation and emplacement.

The production of small volumes of felsic melt in conjunction with hornblende breakdown and garnet formation in hydrous mafic protoliths is explained by phase relations derived from a number of experimental and theoretical studies (cf. Wyllie and Wolf, 1993). Figure 6 shows the major phase boundaries derived from this review for the dehydration partial melting of a hydrous basaltic protolith, or amphibolite. Also shown on Figure 6 is the water-saturated basaltic-andesite liquidus and its slightly water-undersaturated phase boundaries (Stern et al., 1981). Superimposed on the Figure 6 phase relations are the thermobarometric data points and the field of Al-in-hornblende pressure determinations and coupled zircon saturation temperatures (after Watson and Harrison, 1984; Pickett, 1991; Pickett and Saleeby, 1993). The Al-in-hornblende and coupled zircon temperature field is interpreted to represent the initial solidus conditions that were attained during ca. 115–110 Ma and ca. 105–99 Ma lower crustal construction. Below we discuss supra- and subsolidus phase relations and thermobarometric relations that are used to trace out a preferred pressure-temperature path for the high-temperature history of the complex.

The modally dominant early-liquidus phase of the complex is hornblende, which is abundant in Bear Valley suite cumulates, orthogneiss mafic layers, and in commingled dikes and inclusion swarms throughout both the gneisses and Bear Valley suite. Such hornblende-rich cumulates are common, although volumetrically subordinate, throughout the entire Sierra Nevada batholith (cf. Saleeby and Sharp, 1980; Sisson et al., 1996; Clemens-Knott and Saleeby, 1999). At relatively shallow crustal levels (<5 kbar), hornblende is commonly joined by olivine as a cumulate phase, while orthopyroxene ± clinopyroxene are common but subordinate cumulate phases throughout the entire observed depth range for the Sierra Nevada batholith. Garnet occurs only in such mafic cumulates of the Tehachapi complex. The dominance of hornblende as an early liquidus phase is considered a reflection of high water activities in the mantle wedge source for the Sierra Nevada batholith, a feature common to all or most arc environments (cf. Gaetani and Grove, 2003). Stabilization of hornblende as an early liquidus phase in such systems is shown along the water-saturated liquidus of Figure 6. In Figure 6, we diagrammatically show a preferred supra- to hot subsolidus *P-T* path for the Tehachapi complex. The high end of this path is based on the virtual absence of olivine throughout the complex and the dominance of cumulate hornblende ± pyroxenes. The high-*P* end of the suprasolidus path is constrained by igneous garnet-hornblende-poor tonalites and quartz diorites, one of which yields the highest *P-T* values determined for the complex at ~17.4 kbar and ~950 °C. The preferred suprasolidus path is shown to reach solidus conditions at the field defined by the Al-in-hornblende barometry and the zircon saturation temperatures. Fractionation of the mafic cumulates at these conditions left the resulting gabbroids separated from their stabilizing water-rich magma source, which presumably continued ascending higher into the crust. Water activities of 0.01–0.05 typify the migmatitic gabbros (Pickett and Saleeby, 1993).

The preferred hot subsolidus path of the complex is constrained by garnet-based thermobarometry and the "garnet in" line of the hornblende dehydration partial melting reaction (Fig. 6). Water activities were low, as discussed above, and under such conditions two potential components of the subsolidus *P-T* trajectory of the complex are considered to have driven low degrees of dehydration partial melting. First, inspection of the preferred solidus field for the complex and the "garnet in" boundary shows that isobaric cooling could initiate small degrees of partial melting. Second, as suggested by the Figure 4 barochronometric relations, the complex may have been undergoing crustal thickening during Bear Valley suite magmatism, prior to rapid decompression and cooling commencing at ca. 97 Ma. Crustal thickening in the ca. 110–100 Ma time interval is also suggested by the near-penetrative high-temperature ductile deformation fabrics of the gneisses, which also occur locally in the Bear Valley suite. Dehydration partial melting along a cooling versus warming trajectory extending from the preferred solidus field is also indicated by the observed phase relations of clinopyroxene not forming with garnet as a residual phase (Fig. 6).

The hot subsolidus cooling path of the complex is shown to follow an increasing and then decreasing pressure course. Cooling, in conjunction with increasing pressure, initiated low degrees of dehydration partial melting in the hornblende gabbroids. For the temperature range represented by the bulk of the thermobarometric data, Wolf and Wyllie (1994) report 2%–3% melt production via hornblende dehydration and limited melt mobility, similar to that which is widely observed in the migmatitic gabbros. Notable exceptions to such low melt fractions occur locally where more volumetric leucosomes contain pegmatitic lenses or domains (cf. Fig. 5C). The local occurrence of pegmatitic zones in the leucosomes, as well as widespread emplacement of pegmatite dikes coincident with the dehydration partial melting of the gabbros, indicates variable water activities. This is also demonstrated by direct measurements of water activities, which as noted above for the migmatitic gabbros are quite low, but for tonalites and paragneisses are higher and quite variable (Pickett and Saleeby, 1993).

Figure 5. Field photographs showing textural and mesoscale structural relations of garnet formation by dehydration partial melting of mafic cumulates of the Bear Valley intrusive suite. A: Sample 1 trondhjemitic leucosome mantling 1 × 2 cm garnet porphyroblasts within residual hornblende gabbro matrix. B: Sample 5 leucosome and garnet porphyroblast development in hornblende diorite matrix. Arrow denotes fracture mantled with leucosome + garnet. C: Extensive leucosome development in hornblende diorite adjacent to sample 5 site; leucosome material along bottom grading into fractured and poorly exposed trondhjemitic pegmatite of sample 5b. D: Lenticular development of leucosome and garnet porphyroblasts in sample 15. Arrows denote sharp extension fractures filled with garnet. More complex fracture forms are displayed in center area of field.

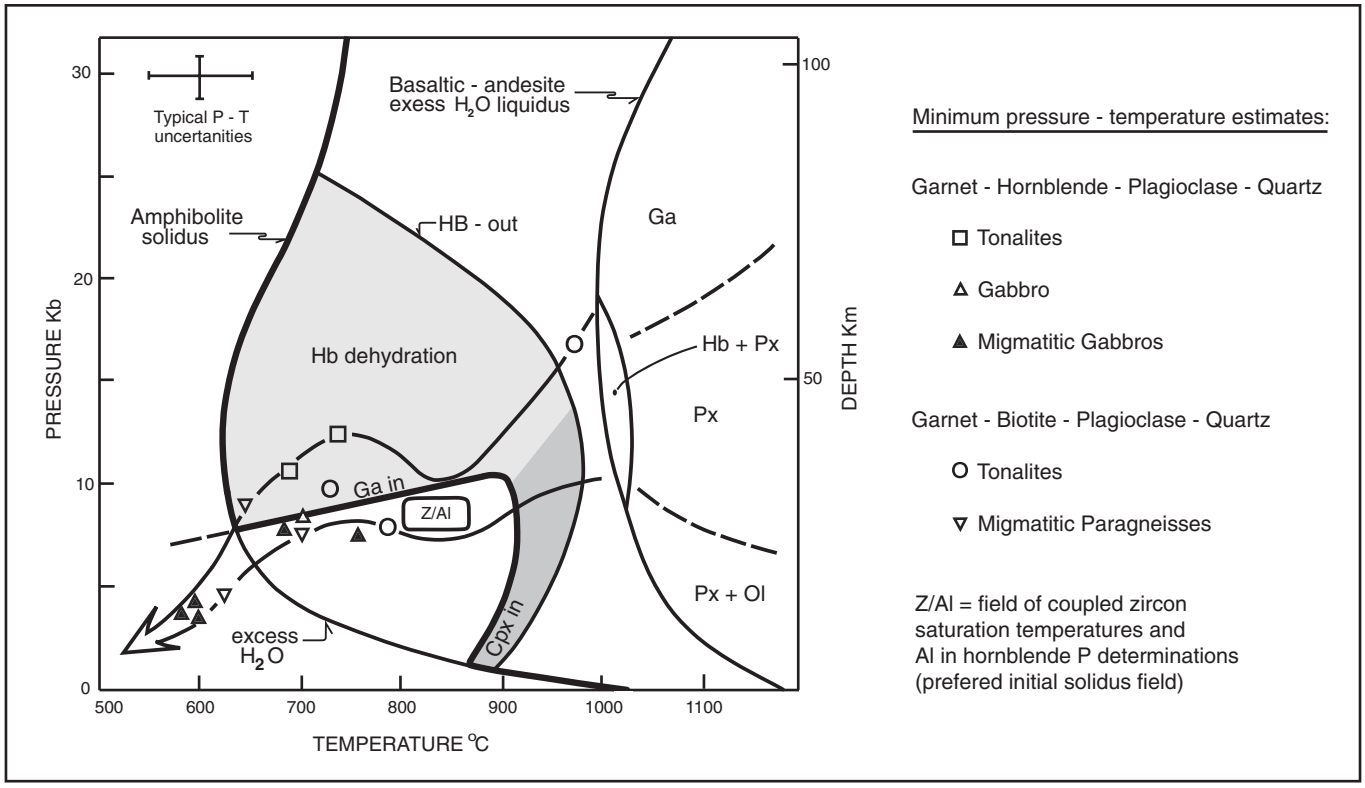

Figure 6. Pressure-temperature plot showing thermobarometric data (Pickett and Saleeby, 1993) plotted onto phase relations of dehydration partial melting of amphibolite (Wyllie and Wolf, 1993) as a proxy for hornblende-rich cumulates of Tehachapi complex, and the water-saturated liquidus for a nominal basaltic-andesite composition along with near-water-saturated phase boundaries (after Stern et al., 1981). The field marked Z/Al is the preferred initial solidus state of the Tehachapi complex based on Al-in-hornblende barometry and zircon saturation temperatures discussed in text. The large arrow demarks our preferred supra- to hot subsolidus path for the complex as discussed in text. Cpx—clinopyroxene; Ga—garnet; Hb—hornblende; Ol—olivine; Px—pyroxene.

A key structural relation in the analysis of water activities during migmatization lies in the high-temperature fracture system that formed in conjunction with migmatization. A number of these fractures have sharp straight edges and exhibit offset patterns in truncated protolith features indicating origin by brittle extension. They are commonly mantled with thin veneers of restitic garnet (Fig. 5D) and/or local thin lenses of leucosome. Leucosome-bearing fractures typically have more diffuse boundaries, with the felsic material grading into the residual matrix (Fig. 5B). Such fractures also appear to have been instrumental in the channeling of externally derived pegmatite dikes. Laboratory studies suggest that positive volume changes during hornblende dehydration partial melting can effectively reduce normal stresses and induce such brittle fracture (cf. Connolly et al., 1997; Rushmer et al., 2003). Extensional fracturing of the partially melting gabbros is suggested to have partially opened up the generally dry local environment to higher-water-activity sources, which resulted in the development of local pegmatitic leucosomes and/or the emplacement of externally derived water-saturated pegmatitic magmas.

The point of the above discussion is to develop a rationale to interpret the lowest *P-T* data points used to constrain the preferred path on Figure 6. This is important in that our barochronometric analysis is strongly dependent on these data points. It is suggested that hornblende dehydration partial melting was instigated in mafic cumulates throughout the complex immediately following intercumulate crystallization via slow cooling with increasing pressure. At ca. 97 Ma, this system began rapid decompression related to tectonically driven exhumation. The thermal response of accelerated cooling initially lagged behind the pressure drop, and thus initial assent was near adiabatic. Rapid decompression also conceivably promoted greater interconnectivity of the high-temperature fracture system, promoting local fluid fluxes and possibly prolonging the molten state of some leucosomes. Under these conditions, the leucosomes remained in a molten state until an appropriate cooling response propagated into the ascending complex. Overall, cooling was faster in the western domain, which relative to the eastern domain was at lower integrated initial temperatures due both to a lower proportion of Bear Valley intrusives and to the regional eastward migration pattern in Sierra Nevada batholith magmatism (Fig. 3). Garnet thermobarometers and Sm/Nd systems for migmatitic gabbro samples 1 and 5 of the western domain were accordingly set at ~7.4 kbar and ca. 97–96 Ma.

The lowest pressures of the complex (~4 kbar) are for migmatitic gabbros of the Tunis Creek area and the nearby

migmatitic paragneiss of El Paso Creek. The Tunis Creek samples also have features indicating low degrees of hornblende dehydration partial melting (Fig. 5D), although pegmatitic leucosome patches that are also present in the gabbro indicate at least local high water activities. The adjacent paragneiss unit is pervasively migmatitic with both amphibolite and granulite facies melanosomes, and it is extensively assimilated along with orthogneisses by the Bear Valley suite tonalite that separates the paragneiss from the Tunis Creek gabbro (Fig. 1). Also, nearby granulitic paragneiss enclaves in the northeasternmost exposures of the Pastoria Creek unit show high-temperature retrograde reactions involving high water activities (Pickett and Saleeby, 1993). Thus the Tunis Creek to El Paso Creek area of the eastern domain appears to have had both a relatively high thermal inertia and highly variable water activity during the initiation of rapid decompression. It is therefore likely that leucosomes encased in the eastern domain remained molten and/or very close to their solidi for an extended period of time relative to those of the western domain. Under these conditions, the complex had decompressed to ~4 kbar by the time (ca. 95 Ma) the cooling response closed the garnet thermobarometric and Sm/Nd systems in the eastern domain.

Exhumation

On the pressure-time plot of Figure 4, a preferred curvilinear path is shown for the garnet data that encompasses a modest increase in pressure between ca. 102 and 99 Ma, followed shortly by rapid decompression. The alternative linear analysis of the data does not take into account petrogenetic aspects of the thermobarometers used, nor the coupling of the thermobarometric and chronometric data. These considerations suggest that the steep decompression path segment between samples 1 and 5 and sample 15 may be more accurate, and that decompression is more readily explained as having occurred in conjunction with rapid cooling. This segment of the path yields a decompression rate of ~2 kbar/m.y., which translates into an overburden exhumation rate of ~7 mm/yr for ~2.5 m.y. between ca. 97 and 93 Ma. This rapid exhumation event is correlated below with the tectonics of Rand Schist underplating.

TECTONICS OF COOLING, EXHUMATION, AND SCHIST UNDERPLATING

Integration of published thermobarometric data with the thermochronometric data presented here reveals a profound decompression and cooling event for the Tehachapi complex at ca. 97–93 Ma and continued rapid cooling with or without decompression until ca. 90–85 Ma. Such a pronounced event resulting in kbar/m.y.- and 100s °C/m.y.-scale decompression and cooling signals a tectonic driving mechanism. Structural relations and geochronologic constraints reviewed below indicate a direct link between this event and the tectonic underplating of the Rand Schist.

Underplating of the Rand Schist and Exhumation of the Tehachapi Complex

Critical time constraints on the underplating of the Rand Schist and the deformation and cooling of the basal domain of the Tehachapi complex are plotted on the time-temperature plot of Figure 7. These constraints are compared on this plot to the preferred cooling path for the chief domains. The solidus to ~200 °C segment of this path is synthesized from the Figure 2A and 2B plots. The low-temperature history of the path is constructed from apatite fission track and (U-Th)/He data for the western domain (Fig. 2A), and from stratigraphic constraints. The absolute constraint for surface exposure of the complex is provided by the middle Eocene nonconformity (Nilsen, 1987). Possible surface exposure in Paleocene time, however, is suggested by remnants of terrestrial and marine locally derived clastic strata that lie nonconformably on southern Sierra basement rocks to the east of the study area (Cox, 1987; Wood and Saleeby, 1998). The basal domain data points shown on the plot include Ar/Ar hornblende and biotite for the sample 17c mylonite, and biotite Ar/Ar and Rb/Sr data and He-zircon data from samples 16, 18, and 19. The sample 16 data are included on the basis of structural relations discussed above in conjunction with their coupled offset pattern from biotite Ar/Ar and Rb/Sr ages of the chief domains. Data points for the Rand Schist include Ar/Ar muscovite and biotite ages as well as a *t-T* path synthesized from the literature. We focus first on the schist path.

The dominant protolith for the Rand Schist is a metaclastic turbidite sequence derived from a Cretaceous magmatic arc source. U/Pb ages for detrital zircon carried in the metaclastics in the Tehachapi Range area indicate a predominately middle to Early Cretaceous age for the arc source, which yielded detrital grains as young as ca. 93 Ma (Grove et al., 2003). This poses a maximum protolith age constraint for at least part of the schist. Convergence rates were ~100 mm/yr in middle to Late Cretaceous time along the southern California margin (Engebretsen et al., 1985), potentially leading to 100 km scale underthrusting in as little as ~1 m.y. The Rand Schist was synkinematically metamorphosed under high-pressure greenschist to epidote amphibolite facies during its underthrusting (Jacobson et al., 1988; Jacobson, 1995). Thermobarometric data for the schist in the Tehachapi Range yield pressures of 8.2–9.7 kbar and temperatures of 590–680 °C (Sharry, 1981; Pickett and Saleeby, 1993). Muscovite and biotite Ar/Ar cooling ages of ca. 90 and ca. 86 Ma, respectively, have been determined for the Tehachapi Range schist (Grove et al., 2003). These ages along with the *P-T* conditions of schist metamorphism, the ca. 92 Ma upper age limit for schist underplating, and the ca. 93 Ma protolith constraint are used to construct a time-temperature path for the schist. The cooling segment of this path is constrained to be even steeper than that of the gneiss complex, and appears to converge with the gneiss curve within the biotite closure temperature field. Such a condensed subduction and cooling history for the schist sharply diverges from steady-state conditions that are expected in sub-

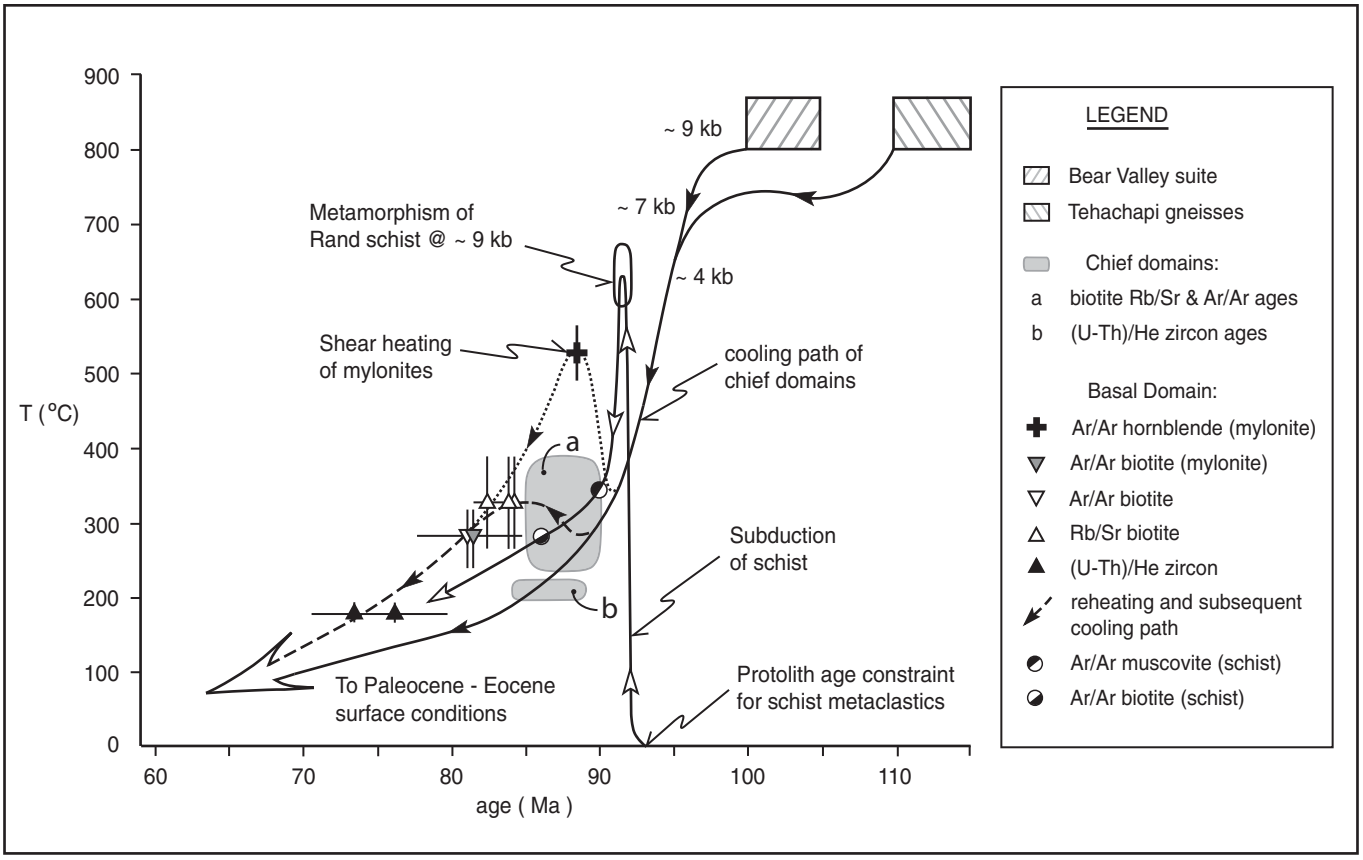

Figure 7. Time-temperature (*t-T*) plots for thermochronometric data from samples interpreted to have been reheated during tectonic underplating of Rand Schist along basal domain (sample 16 biotite Rb/Sr and Ar/Ar, 17c mylonite, 18, and 19). Preferred cooling path for chief domains of complex are derived from Figures 2A and 2B, as well as principal fields of biotite Rb/Sr and Ar/Ar and He-zircon closure. Corresponding decompression path for complex is denoted by kbar values along cooling curve. Note that slower cooling rate closure temperature is used for basal domain He-zircon data (Table 1). Also shown are Ar/Ar muscovite and biotite data, protolith age constraints (Grove et al., 2003), equilibrium pressure-temperature conditions of metamorphism (Pickett and Saleeby, 1993), and derivative time-temperature path of for Rand Schist.

duction zones based on thermal modeling (Peacock, 1992). We pursue this problem further by considering structural and thermal relations along the basal domain.

The basal domain of the Tehachapi complex lies along the north branch of the Garlock fault, encompassing much of the White Oak unit and the immediately adjacent parts of the Bison Peak, Tejon Creek, and Pastoria Creek units. Mylonite zones are common in this domain, and in the White Oak unit mylonitization is more pervasive and is commonly overprinted and retrograded to chlorite phyllonite and cataclasite. The mylonitization and retrograde zones are related to the Rand fault. Such tectonized and altered zones also occur in discrete domains throughout the complex, particularly adjacent to small windows into the underlying schist. Samples 17–19 are from the basal domain. In the area of sample 17, the Tejon Creek unit grades into the White Oak unit by picking up domainal mylonite zones that are superimposed over higher-grade crystalloblastic fabrics. Sample 17c is from a relatively pristine mylonite zone within the Tejon Creek unit ~200 m from the White Oak contact. The high-strain zone is ~5 m wide, having relatively steep strain gradients (centimeters) with its tonalitic protolith. Hornblende in the mylonite is porphyroclastic with finely chloritized rims and tails, while biotite is highly deformed into fine lamina with chlorite intergrowths, and oriented along slip surfaces. Ar/Ar hornblende and biotite, and Rb/Sr biotite dates of ca. 89 Ma, ca. 81 Ma, and ca. 74 Ma respectively, were determined for the mylonite. Nonmylonitized tonalite gneiss collected ~15 m from the mylonite zone yields a ca. 85 Ma Ar/Ar biotite age, and the adjacent meter-scale amphibolitic diorite layer yields an Ar/Ar hornblende age of ca. 93 Ma (samples 17 and 17b respectively). Mylonitization has clearly affected the Ar/Ar and Rb/Sr systems of sample 17 site.

The hornblende and biotite Ar/Ar age data for the sample 17c mylonite are plotted on Figure 7. The Rb/Sr biotite data for this sample are omitted based on suspected chemical alteration effects discussed earlier. Hornblende closure in the mylonite was synchronous with muscovite Ar/Ar closure in the underlying schist. However, the biotite Ar/Ar and Rb/Sr systems throughout the chief domains of the complex were also set at about the

same time that the mylonite hornblende was set. Textural relations indicate that grain size reduction was not a major factor in the mylonite hornblende closure temperature. These relations suggest that the mylonite zone was heated nearly 200 °C by concentrated shearing at ca. 89 Ma. The thermal effects of such shearing are shown to be concentrated within the mylonite zone, in that relatively pristine hornblende just ~15 m from the edge of the zone (sample 17b) retains the ca. 93 Ma Ar/Ar age as is typical throughout the complex. Extreme grain size reduction in the biotite may be invoked to yield the younger biotite ages. Calculations of Ar closure temperatures versus diffusion radii in mylonitized biotites indicate that grain size reduction begins to play a significant role at radii below ~50 μm (Goodwin and Renne, 1991). This is pertinent for the sample 17c biotite, which is deformed into fine sheaths, many of which are substantially less than ~50 μm in thickness. The 17c biotite is the only sample that did not yield a plateau age, which could be related to such severe grain size reduction. Samples 18 and 19 are from the Tejon Creek and Bison Peak units as they grade into the basal domain. Both sample sites exhibit protomylonitic fabrics that intensify southward into the White Oak unit. Sample 18 yields a ca. 84 Ma Rb/Sr biotite age and a ca. 76 Ma He-zircon age. Sample 19 yields a Rb/Sr biotite age of ca. 82 Ma and a He-zircon age of ca. 73 Ma. These data are plotted on Figure 7 apart from the chief biotite and He-zircon fields and are discussed further below.

An important feature of the cooling curves shown for the Rand Schist and the Tehachapi complex on Figure 7 is that at the time of schist underthrusting to ~9 kbar conditions (ca. 90 Ma) the Tehachapi complex had already been decompressed to ~4 kbar conditions. Thus, relative to conditions set at roughly 90 Ma, the juxtaposition of the schist against the gneisses encompasses an ~4 kbar equivalent section of missing rock. This pressure juxtaposition is constrained in age by the Late Cretaceous to Paleocene southern Sierra detachment system locally cutting out the gneisses and placing high-level detachment sheets directly onto the schist (Wood and Saleeby, 1998; Saleeby and Foster, 2004). The coincidence of the muscovite and biotite Ar/Ar ages for the schist with the chief cluster of biotite ages for the gneiss complex may approximate the convergence time for pressures and thus crustal levels for the schist and gneisses. However, such a convergence should be most clearly expressed along the basal domain. Basal domain biotite as well as He-zircon ages are distinctly younger than those of both the chief domains and the schist.

The pressure-temperature-time relationships displayed between the Tehachapi complex and the Rand Schist on Figure 7 speak to a long-standing problem concerning all of the major lower-plate schist bodies of the southern California region. Examples of deep crustal ductile thrust contacts between the schists and their overlying batholithic plates, presumably recording subduction of the schist, are rare. A number of ductile to brittle low-angle structures that could be interpreted as the remnants of such thrusts yield contrary kinematic indicators to regional-scale east-directed underthrusting (Ehlig, 1981; Nourse, 1989; Jacobson et al., 1988). The mylonite zones along the basal domain of the Tehachapi complex, like that of sample 17c, for the most part record horizontal extension with only local evidence of noncoaxial strain. The few examples of well-developed noncoaxial strain that have been located suggest that the schist has moved generally southwestward relative to the Tehachapi complex. These observations in conjunction with the pressure-temperature-time relations of Figure 7 suggest that the schist was decompressed and cooled as it moved by low-angle normal-sense displacement from beneath the southernmost Sierra Nevada batholith. The sample 17c mylonite Ar/Ar hornblende age of ca. 89 Ma in this interpretation records shear related to such normal displacement along the Rand fault. As the schist ascended, it is suggested to have advected heat into the basal domain, thereby resetting the biotite and He-zircon ages of samples 18 and 19. Partial resetting of the sample 17a biotite ages may have occurred as well, considering that these ages lie at the lower end of the cluster of Ar/Ar and Rb/Sr ages for the chief domains (Table 6). Reheating of the basal domain by shear appears to be of second-order importance except as restricted to mylonite zones, considering the relationships between the sample 17a and 17b biotite and hornblende ages versus the immediately adjacent 17c mylonite ages. In this interpretation, a crustal-level convergence time of ca. 80 Ma is favored for the schist and gneiss complex. This would imply a minimum decompression rate of ~0.5 kbar/m.y. for the schist as it ascended. A faster rate is implied if the upper-plate gneiss complex was still ascending to higher crustal levels while the schist was ascending and converging with it. This seems likely in that the gneiss complex ascended from ~4 kbar levels to surface levels in the interval between ca. 94 Ma and Paleocene to middle Eocene time (ca. 65–52 Ma).

Seismic reflection data image the Rand fault dipping at shallow angles beneath the lower El Paso to Tejon Creek area, and steepening to ~30°N dips beneath the Tejon Embayment (Malin et al., 1995). Map relations suggest that the fault has significant structural relief, at least in part imposed by Neogene-Quaternary deformation. The sample 16 biotite Ar/Ar and Rb/Sr age data much more closely resemble basal domain data than those of the chief domains (Table 6). Sample 16 lies adjacent to the Tejon Canyon lineament. Such lineaments and related fracture systems are under investigation regionally with pursuit of their potential origin in conjunction with the extensional denudation of the oblique crustal section. A tentative interpretation of the sample 16 structural relations is that the Rand fault shallows beneath the sample site, and the upper plate in this area was reheated, as in the basal domain, and broken by extensional shear fractures that subsequently localized the Tejon Canyon lineament.

Tectonics of Schist Underplating and Tehachapi Complex Exhumation

The ~5 m.y. time lag between rapid cooling and decompression of the gneiss complex and schist underplating is an important tectonic signal. Prior to the tectonic underplating of the schist, the lowermost crust and mantle wedge that formed

beneath the southernmost Sierra Nevada batholith and adjacent northern Mojave batholith was removed. This subbatholithic section is reasonably well constrained in its composition, age, and petrogenesis by studies of mantle xenoliths that were entrained in Neogene lavas erupted through the central Sierra Nevada batholith (Ducea and Saleeby, 1996, 1998). The deep batholithic section of the Tehachapi complex may be mated to the greater Sierra Nevada batholith mantle wedge section based on the convergence of rock types and on the thermobarometrically determined mantle geotherm intersecting the peak pressures and temperatures determined for the Tehachapi complex (Saleeby et al., 2003) (Fig. 2). According to the xenolith data, the subbatholith Moho was only an equivalent of ~2 kbar deeper than the ~9–10 kbar level that the Tehachapi complex formed at, and the base of the mantle wedge peridotites extended to a minimum depth of ~125 km. Thus at least an ~90 km section of mantle lithosphere as well as a veneer of lowermost crust was removed from beneath the Tehachapi complex prior to schist underplating.

Mantle lithosphere removal from beneath the Tehachapi complex is interpreted to have resulted from tectonic erosion by an abrupt flattening in the subduction trajectory of the Farallon plate as it entered the southern California region subduction zone (Malin et al., 1995; Saleeby, 2003). Subduction flattening has been hypothesized for Late Cretaceous time beneath the southwestern Cordillera as a mechanism for driving the Laramide orogeny of the plate interior (Coney and Reynolds, 1977; Dickinson and Snyder, 1978). These and other similar flat slab models rely on changes in Farallon plate age or velocity as a flattening mechanism. Such a mechanism has difficulty explaining the abruptness with which the southernmost Sierra Nevada batholith was disrupted, and in particular the abruptness with which the Tehachapi complex was exhumed, cooled, and underplated by the schist. A second class of models for "Laramide flat slab subduction" focuses more on the details of its plate margin manifestations including the restricted locus of batholithic belt disruption and schist underplating, and on the structure of the abyssal lithosphere that was subducted in the California region at Laramide time (Livaccari et al., 1981; Henderson et al., 1984; Tarduno et al., 1985; Barth and Schneiderman, 1996; Saleeby, 2003). The Farallon lithosphere at this time contained the conjugate massif to the Hess-Shatsky Rise of the northwest Pacific basin, which subducted along an anomalously shallow trajectory beneath the southwestern Cordillera due to the added buoyancy of its thickened crustal section. In doing so, it disrupted the corresponding segment of the California margin. The Tehachapi complex lies along the northern margin of this flat slab segment damage zone. Consequently, the subbatholith mantle lithosphere remained intact throughout the greater Sierra Nevada batholith to the north, to be sampled as xenoliths in Neogene lavas. In parallel, there are no signs of schist underplating to the north, and the Great Valley forearc basin, except in the extreme south adjacent to the Tehachapi Range, has remained intact.

The Rand Schist is a member of a family of similar schists of the southern California region that lie in similar anomalous positions tectonically beneath a distinct disrupted segment of the regional batholithic belt. The along-strike extent of the schists and their upper batholithic plates are thought to approximate the limits of the plate margin zone that experienced the effects of the flat slab segment. U/Pb geochronological studies of detrital zircon from metaclastic units of the various schist bodies along this distinct segment of the Mesozoic margin reveal a similar pattern to that which was discussed above for the Tehachapi Range: rapid dissection of the proximal magmatic arc and delivery of the derivative first-cycle detritus to the subducting trench, and then rapid subduction and underplating beneath the adjacent arc segment at roughly sub-arc Moho depths (Barth et al., 2003; Grove et al., 2003).

Reviewing the temporal relations in Figure 7 between gneiss complex cooling/decompression and schist underplating/cooling in the context of the regional tectonics discussed above, the following tectonic history may be derived. Southwestern Cordilleran arc magmatism maintained a regionally coherent pattern from at least the Sierra Nevada through the Peninsular Ranges batholiths into middle Cretaceous time. Between ca. 110 and 105 Ma, subduction parameters along the entire North American batholithic belt changed to a more highly coupled state, which resulted in widespread intra-arc shortening, crustal thickening, and the beginning of a more coherent eastward migration pattern in arc magmatism (Silver et al., 1979; Todd et al., 1988; Rubin and Saleeby, 1992; Tobisch et al., 1995; Ducea, 2001). This change is manifest in the Tehachapi complex by near-pervasive high-temperature deformation fabrics in the gneisses and more locally in the Bear Valley suite, ca. 102–99 Ma crustal thickening, and eastward migration in magmatism. At ca. 98 Ma and at the position of the southernmost Sierra Nevada batholith and northern Mojave batholith, the northern margin of a shallow slab segment in the Farallon plate, presumably the Hess-Shatsky Rise conjugate, entered the subducting trench and began a rapid destructive trajectory through the forearc and beneath the still-active arc. The forearc and mantle wedge were tectonically eroded as rapid uplift, decompression, and partial exhumation of the Tehachapi complex occurred. Partial exhumation of the upper crust occurred by a combination of tectonic denudation, discussed further below, and vigorous erosion. Copious arc-derived detritus was shed into the subducting trench, some of which was displaced down the shallow subduction zone and underplated beneath the disrupted magmatic arc. The greater Sierra Nevada batholith arc-generated lithosphere remained intact to the north, but the western Mojave Desert and adjacent areas of the arc for an along-strike distance of ~500 km were severely disrupted and underplated by the schist as beneath the Tehachapi complex. Seismic reflection data that show the schist dipping northward beneath the Tehachapi complex (Malin et al., 1995) are interpreted to image the remnants of the along-strike inflection in the Farallon slab from the shallow southern to northern deeper segments. The regional tilt of the southernmost Sierra Nevada batholith oblique crustal section complements the seismically imaged dip of the inflection zone (Saleeby et al., 2003; Saleeby, 2003).

The abruptness with which the schist was subducted and then transported back to significantly shallower crustal levels requires special attention. In the analysis offered above, a vigorous phase of terminal low-angle normal displacement is hypothesized for the Rand fault. Temporal relations of the southern Sierra detachment system indicate that the upper crust above the Rand fault also underwent high-magnitude extensional faulting coincident with its normal displacement phase. Such upper crustal extension resulted in the transport of relatively high-level eastern Sierra Nevada batholith–affinity rocks southward and westward down onto the deeper-level rocks of the Tehachapi complex. Thus, following the tectonic erosion of the mantle wedge and the underthrusting of the schist by shallow subduction, the residual crust of the complex was abruptly attenuated by regional extension. Characteristic dimensions of the Hess-Shatsky Rise (Iwabuchi, 1984), in conjunction with Farallon plate subduction rates referenced above, suggest that a roughly symmetrical conjugate to the rise would interact for only ~10 m.y. at any reference point along its subduction trajectory. It has been hypothesized that a steepening in subduction angle of the shallow slab segment should follow in the wake of the rise conjugate as normal abyssal lithosphere resumed its descent into the subduction zone. This would in effect induce a slab rollback effect behind the shallow slab segment, thereby pulling an extensional flow channel in the underplated schist, causing it to fill back into the opening forearc region. Such a basal crust flow channel is suggested at regional scales to have induced upper-plate extension by traction along the base of the upper plate, and not only to have resulted in the pronounced extensional event resolved in the Tehachapi complex, but to have likewise affected the entire plate edge damage zone above the shallow slab segment (Saleeby, 2003). One of the clearest regional structural manifestations of this flow pattern is the westward deflection pattern observed in the southern California region batholithic belt when restored to its pre-Neogene configuration. Locally, this is expressed by the westward deflection and clockwise rotation of the Sierra Nevada batholith as it deepens into the Tehachapi complex (Fig. 1).

CONCLUSIONS

Thermochronometers hosted in garnet, titanite, hornblende, biotite, and zircon record the cooling history of the Tehachapi complex commencing at high-volume batholith solidus conditions, and descending to low-grade conditions below ~170 °C. The thermochronometric data array could be interpreted to record a rapid constant cooling rate of ~35–40 °C/m.y., but a nonlinear cooling path with both faster and slower segments is favored when the data are interpreted in the context of barochronometric, petrogenetic, and regional tectonic constraints. The Tehachapi complex formed at ~8–10 kbar conditions by copious arc magmatism that culminated at ca. 100 Ma. It began a slow conductive cooling path in the wake of the regional eastward migration of arc magmatism that typified the Cretaceous North American Cordilleran batholithic belt. Along the southern California segment of this belt, the Late Cretaceous subduction of the conjugate massif to the Hess-Shatsky Rise resulted in a flat slab subduction regime that in the southernmost Sierra Nevada batholith region lasted <10 m.y. Such slab flattening in this region began at ca. 98 Ma, disrupted the entire forearc region, and propagated beneath the western margin of the arc by ca. 97 Ma. It tectonically eroded away the corresponding forearc and mantle wedge, and drove rapid exhumation at a rates of ~7 mm/yr between 97 and 93 Ma. Cooling rates during this time interval may have briefly peaked as high as ~500 °C/m.y. Garnet Sm/Nd, titanite U/Pb, and hornblende Ar/Ar systems in the complex were set during this time interval. Starting at ca. 93 Ma, cooling rates slowed to the ~40 °C/m.y. rate, and exhumation slowed to an unknown rate. Biotite Rb/Sr and Ar/Ar systems and He-zircon systems were set along this segment of the cooling path. At <200 °C and ca. 85 Ma, cooling rates slowed markedly with poorly constrained exhumation rates, but ultimately the complex reached surface conditions prior to middle Eocene marine nonconformable overlap (ca. 52 Ma).

Rapid exhumation of the southernmost Sierra Nevada batholith region resulted in the production of an extensive arc-derived sand sheet that was shed into the subducting trench. Derivative clastic strata were subducted at low angles beneath the southern Sierra Nevada batholith, metamorphosed in high-pressure greenschist-amphibolite facies, and along with fragments of subducted abyssal lithosphere transformed into the Rand Schist. Peak metamorphism of the Rand Schist occurred at ca. 90 Ma and at ~590–680 °C and ~9 kbar conditions. The upper-plate Tehachapi complex had already been decompressed down to ~4 kbar conditions, deeply exhumed, and cooled to biotite Rb/Sr and Ar/Ar temperatures at the time that the Rand Schist reached its peak conditions. Between 90 and 88 Ma, the schist began a rapid tectonic ascent by low-angle normal displacement along the previous subduction thrust system, and by ca. 80 Ma it was underplated at its current structural position beneath the Tehachapi complex. The Tehachapi complex and mid-crustal Sierra Nevada batholith rocks in proximal regions to the north were further exhumed by tectonic denudation of the southern Sierra detachment system that worked in concert with underlying normal displacement along the Rand fault. The southward-deepening exhumation pattern cut an oblique crustal section through the southernmost Sierra Nevada batholith. The crustal section and the deeply exhumed Tehachapi complex are the crustal-level expression of a Late Cretaceous inflection in the Farallon plate where the dip of subduction abruptly shallowed to the south.

ACKNOWLEDGMENTS

This research was funded by National Science Foundation grants EAR-9526859 and EAR-0087347 (to J.S.), and EAR-0230383 (to J.S. and K.F.), and the Gordon and Betty Moore Foundation. This is Caltech Tectonic Observatory Contribution number 49. This research benefited from discussions and field excursions with M. Ducea, L.T. Silver, R.K. O'Nions, P.D. Asimow, D.A. Pickett, D.J. Wood, P.J. Wyllie, and J. Eiler. Field, laboratory, and

computational assistance by L. Hedges, E. Nadin, and Z. Foster-Saleeby and assistance in manuscript preparation by Kim Klotz are kindly acknowledged. Limited access to private lands held by the Tejon Ranch Company is gratefully acknowledged.

REFERENCES CITED

Ague, J.J., 1997, Thermodynamic calculation of emplacement pressures for batholithic rocks, California: Implication for the aluminum-in-hornblende barometer: Geology, v. 25, p. 563–566, doi: 10.1130/0091-7613(1997)025<0563:TCOEPF>2.3.CO;2.

Ague, J.J., and Brimhall, G.H., 1988, Magmatic arc asymmetry and distribution of anomalous plutonic belts in the batholiths of California: Effects of assimilation, crustal thickness, and depth of crystallization: Geological Society of America Bulletin, v. 100, p. 912–927.

Anderson, J.L., and Smith, D.R., 1995, The effects of temperature and fO_2 on the Al-in-hornblende barometer: American Mineralogy, v. 80, p. 549–559.

Barazangi, M., and Isacks, B., 1976, Spatial distribution of earthquakes and subduction of the Nazca plate beneath South America: Geology, v. 4, p. 686–692, doi: 10.1130/0091-7613(1976)4<686:SDOEAS>2.0.CO;2.

Barth, A.P., and Schneiderman, J.S., 1996, A comparison of structures in the Andean orogen of northern Chile and exhumed midcrustal structures in southern California, USA: An analogy in tectonic style?: International Geological Reviews, v. 38, p. 1075–1085.

Barth, A.P., Wooden, J.L., Grove, M., Jacobson, C.E., and Pedrick, J.N., 2003, U-Pb zircon geochronology of rocks in the Salinas Valley region of California: A reevaluation of the crustal structure and origin of the Salinian block: Geology, v. 31, p. 517–520.

Barton, M.D., and Hanson, R.B., 1989, Magmatism and the development of low-pressure metamorphic belts: Implications from the western United States and thermal modeling: Geological Society of America Bulletin, v. 101, p. 1051–1065, doi: 10.1130/0016-7606(1989)101<1051:MATDOL>2.3.CO;2.

Barton, M.D., Battles, D.A., Bebout, G.E., Capo, R.C., Christensen, J.N., Davis, S.R., Hanson, R.B., Michelsen, C.J., and Trim, H., 1988, Mesozoic contact metamorphism in the western United States, *in* Ernst, W.G., ed., Metamorphism and crustal evolution of the western United States (Rubey Volume VII): Englewood Cliffs, New Jersey, Prentice-Hall, p. 110–178.

Chen, J.H., and Moore, J.G., 1982, Uranium-lead isotopic ages from the Sierra Nevada batholith: Journal of Geophysical Research, v. 87, p. 4761–4784.

Chen, J.H., and Tilton, G.R., 1991, Applications of lead and strontium isotopic relationships to the petrogenesis of granitoid rocks, central Sierra Nevada batholith, California: Geological Society of America Bulletin, v. 103, p. 439–447, doi: 10.1130/0016-7606(1991)103<0439:AOLASI>2.3.CO;2.

Cherniak, D.J., 1993, Lead diffusion in titanite and preliminary results on the effects of radiation damage on Pb transport: Chemical Geology, v. 110, p. 177–194, doi: 10.1016/0009-2541(93)90253-F.

Clemens-Knott, D., and Saleeby, J.B., 1999, Impinging ring dike complexes in the Sierra Nevada batholith, California: Roots of the Early Cretaceous volcanic arc: Geological Society of America Bulletin, v. 111, p. 484–496, doi: 10.1130/0016-7606(1999)111<0484:IRDCIT>2.3.CO;2.

Cohen, A.S., O'Nions, K.R., Siegenthaler, R., and Griffin, W.L., 1988, Chronology of the pressure-temperature history recorded by a granulite terrane: Contributions to Mineralogy and Petrology, v. 98, p. 303–311, doi: 10.1007/BF00375181.

Coleman, D.S., and Glazner, A.F., 1998, The Sierra Crest magmatic event: Rapid formation of juvenile crust during the Late Cretaceous in California, *in* Ernst, W.G., and Nelson, C.A., eds., Integrated earth and environment evolution of the southwestern United States: Columbia, Maryland, Bellwether Publishing, p. 253–272.

Coney, P.J., and Reynolds, S.J., 1977, Cordilleran Benioff zones: Nature, v. 270, p. 403–406, doi: 10.1038/270403a0.

Connolly, J.A.D., Holness, M.B., Rubie, D.C., and Rushmer, T., 1997, Reaction-induced microcracking: An experimental investigation of a mechanism for enhancing anatectic melt extraction: Geology, v. 25, p. 591–594, doi: 10.1130/0091-7613(1997)025<0591:RIMAEI>2.3.CO;2.

Cox, B.F., 1987, Stratigraphy, depositional environments, and paleotectonics of the Paleocene and Eocene Golar Formation, El Paso Mountains, California—Geologic summary and roadlog, *in* Cox, B.F., ed., Basin analysis and paleontology of the Paleocene and Eocene Golar Formation, El Paso Mountains, California: Pacific Section, Society of Economic Paleontologists and Mineralogists Guidebook 57, p. 1–29.

Dahl, P.S., 1997, A crystal-chemical basis for Pb retention and fission-track annealing systematics in U-bearing mineral, with implications for geochronology: Earth and Planetary Science Letters, v. 150, p. 277–290, doi: 10.1016/S0012-821X(97)00108-8.

DePaolo, D.J., 1981, A neodymium and strontium study of the Mesozoic calc-alkaline granitic batholiths of the Sierra Nevada and Peninsular Ranges: Journal of Geophysical Research, v. 86, p. 10,470–10,488.

Dickinson, W., and Snyder, W.S., 1978, Plate tectonics of the Laramide orogeny: Geological Society of America Memoir 151, p. 335–366.

Dodson, M.H., 1973, Closure temperature in cooling geochronological and petrological systems: Contributions to Mineralogy and Petrology, v. 40, p. 259–274, doi: 10.1007/BF00373790.

Ducea, M.N., 2001, The California arc: Thick granitic batholiths, eclogitic residues, lithospheric-scale thrusting, and magmatic flare-ups: GSA Today, v. 11, no. 11, p. 4–10, doi: 10.1130/1052-5173(2001)011<0004:TCATGB>2.0.CO;2.

Ducea, M.N., and Saleeby, J.B., 1996, Buoyancy sources for a large, unrooted mountain range, the Sierra Nevada, California: Evidence from xenolith thermobarometry: Journal of Geophysical Research, v. 101, p. 8229–8244, doi: 10.1029/95JB03452.

Ducea, M.N., and Saleeby, J.B., 1998, The age and origin of a thick mafic-ultramafic keel from beneath the Sierra Nevada batholith: Contributions to Mineralogy and Petrology, v. 133, p. 169–185, doi: 10.1007/s004100050445.

Ehlig, P.L., 1981, Origin and tectonic history of the basement terrane of the San Gabriel Mountains, central Transverse Ranges, *in* Ernst, W.G., ed., The geotectonic development of California: Englewood Cliffs, New Jersey, Prentice-Hall, p. 253–283.

Elphick, S.C., Ganguly, J., and Loomis, T.P., 1985, Experimental determination of cation diffusivities in aluminosilicate garnets, I: Experimental methods and interdiffusion data: Contributions to Mineralogy and Petrology, v. 90, p. 36–44, doi: 10.1007/BF00373039.

Engebretsen, D.C., Cox, A., and Gordon, R.G., 1985, Relative motions between oceanic and continental plates in the Pacific basin: Geological Society of America Special Paper 206, 59 p.

England, P., and Molnar, P., 1990, Surface uplift, uplift of rocks, and exhumation of rocks: Geology, v. 18, p. 1173–1177, doi: 10.1130/0091-7613(1990)018<1173:SUUORA>2.3.CO;2.

Evernden, J.F., and Kistler, R.W., 1970, Chronology of emplacement of Mesozoic batholithic complexes in California and western Nevada: U.S. Geological Survey Professional Paper 623, 42 p.

Farley, K.A., 2000, Helium diffusion from apatite: General behavior as illustrated by Durango fluorapatite: Journal of Geophysical Research, v. 105, p. 2903–2914, doi: 10.1029/1999JB900348.

Farley, K.A., Wolf, R.A., and Silver, L.T., 1996, The effects of long alpha-stopping on (U-Th)/He dates: Geochimica et Cosmochimica Acta, v. 60, p. 1–7.

Fleck, R.J., Criss, R.E., Eaton, G.F., Cleland, R.W., Wavra, C.S., and Bond, W.D., 2002, Age and origin of base and precious metal veins of the Coeur D'Alene Mining District, Idaho: Economic Geology and the Bulletin of the Society of Economic Geologists, v. 97, p. 23–42.

Fliedner, M.M., Klemperer, S.L., and Christensen, N.I., 2000, Three-dimensional seismic model of the Sierra Nevada arc, California, and its implications for crustal and upper mantle composition: Journal of Geophysical Research, v. 105, p. 10,899–10,921, doi: 10.1029/2000JB900029.

Gaetani, G.A., and Grove, T.L., 2003, Experimental constraints on melt generation in the mantle wedge, *in* Eiler, J., ed., Inside the subduction factory: American Geophysical Union Geophysical Monograph 138, p. 107–134.

Ganguly, J., Tirone, M., and Hervig, R., 1998, Diffusion kinetics of samarium and neodymium in garnet, and a method of determining cooling rates of rocks: Science, v. 281, p. 805–807, doi: 10.1126/science.281.5378.805.

Goodwin, L.B., and Renne, P.R., 1991, Effects of progressive mylonitization on Ar retention in biotites from the Santa Rosa mylonite zone, California, and thermochronologic implications: Contributions to Mineralogy and Petrology, v. 108, p. 283–297, doi: 10.1007/BF00285937.

Grove, M., Jacobson, C.E., Barth, A.P., and Vucic, A., 2003, Temporal and spatial trends of Late Cretaceous–early Tertiary underplating of Pelona and related schist beneath southern California and southwestern Arizona: Geological Society of America Special Paper 375, p. 381–406.

Gutscher, M.A., Spakman, W., Bijwaard, H., and Engdahl, E.R., 2000, Geodynamics of flat subduction: Seismicity and tomographic constraints from the Andean margin: Tectonics, v. 19, p. 814–833, doi: 10.1029/1999TC001152.

Hammarstrom, J.M., and Zen, E., 1986, Aluminum in hornblende: An empirical igneous geobarometer: American Mineralogy, v. 71, p. 1297–1313.

Harrison, T.M., 1981, Diffusion of ^{40}Ar in hornblende: Contributions to Mineralogy and Petrology, v. 78, p. 324–331, doi: 10.1007/BF00398927.

Henderson, L.J., Gordon, R.G., and Engebretson, D.C., 1984, Mesozoic aseismic ridges on the Farallon plate and southward migration of shallow subduction during the Laramide orogeny: Tectonics, v. 3, p. 121–132.

Hollister, L.S., Grissom, G.C., Peters, E.K., Stowell, H.H., and Sisson, V.B., 1987, Confirmation and empirical correlation of Al in hornblende with pressure of solidification of calc-alkaline plutons: American Mineralogy, v. 72, p. 231–239.

Iwabuchi, Y., 1984, General bathymetric chart of the oceans (GEBCO), sheets 5.06 and 5.07: Ottawa, Canada, Canadian Hydrographic Services, scale 1:10,000,000.

Jacobson, C.E., 1995, Qualitative thermobarometry of inverted metamorphism in the Pelona and Rand Schists, southern California, using calciferous amphibole in mafic schist: Journal of Metamorphic Geology, v. 13, p. 79–92.

Jacobson, C.E., Dawson, M.R., and Postlethwaite, C.E., 1988, Structure, metamorphism and tectonic significance of the Pelona, Orocopia and Rand Schists, southern California, *in* Ernst, W.G., ed., Metamorphism and crustal evolution of the western United States (Rubey Volume VII): Englewood Cliffs, New Jersey, Prentice-Hall, p. 976–997.

Jacobson, C.E., Oyarzabal, F.R., and Haxel, G.B., 1996, Subduction and exhumation of the Pelona-Orocopia-Rand Schists, southern California: Geology, v. 24, p. 547–550, doi: 10.1130/0091-7613(1996)024<0547:SAEOTP>2.3.CO;2.

Jaffey, A.H., Flynn, K.F., Glendenin, L.E., Bentley, W.C., and Essling, A.M., 1971, Precision measurement of half-lives and specific activities of ^{235}U and ^{238}U: Physical Review, v. C4, p. 1889–1906.

James, E.W., 1992, Cretaceous metamorphism and plutonism in the Santa Cruz Mountains, Salinian block, California, and correlation with the southernmost Sierra Nevada: Geological Society of America Bulletin, v. 104, p. 1326–1339, doi: 10.1130/0016-7606(1992)104<1326:CMAPIT>2.3.CO;2.

Johnston, A.D., and Wyllie, P.J., 1988, Constraints on the origin of Archean trondhjemites based on phase relationships of Nuk gneiss with H_2O at 15 kb: Contributions to Mineralogy and Petrology, v. 100, p. 35–46, doi: 10.1007/BF00399438.

Kanter, L.R., and McWilliams, M.O., 1982, Rotation of the southernmost Sierra Nevada, California: Journal of Geophysical Research, v. 87, p. 3819–3830.

Kistler, R.W., 1990, Two different types of lithosphere in the Sierra Nevada, California: Geological Society of America Memoir 174, p. 271–282.

Kistler, R.W., and Peterman, Z., 1973, Variations in Sr, Rb, K, Na and initial ^{87}Sr/^{86}Sr in Mesozoic granitic rocks and intruded wall rocks in central California: Geological Society of America Bulletin, v. 84, p. 3489–3512, doi: 10.1130/0016-7606(1973)84<3489:VISRKN>2.0.CO;2.

Kistler, R.W., and Ross, D.C., 1990, A strontium isotopic study of plutons and associated rocks of the southern Sierra Nevada and vicinity, California: U.S. Geological Survey Bulletin 1920, 20 p.

Lackey, J.S., Valley, J.W., and Saleeby, J.B., 2005, Supracrustal input to magmas in the deep crust of the Sierra Nevada batholith: Evidence from high-δ^{18}O zircon: Earth and Planetary Science Letters, v. 235, p. 315–330, doi: 10.1016/j.epsl.2005.04.003.

Livaccari, R.F., Burke, K., and Sengor, A.M.C., 1981, Was the Laramide orogeny related to subduction of an oceanic plateau?: Nature, v. 289, p. 276–278, doi: 10.1038/289276a0.

Ludwig, K.R., 1999, User's manual for Isoplot/Ex, version 2.05: Berkeley, California, Berkeley Geochronology Center Special Publication 1a, 48 p.

Ludwig, K.R., 2001, Users manual for Isoplot/Ex (rev. 2.49): A geological toolkit for Microsoft Excel: Berkeley, California, Berkeley Geochronology Center Special Publication 1a, 56 p.

Malin, P.E., Goodman, E.D., Henyey, T.L., Li, Y.-G., Okaya, D.A., and Saleeby, J.B., 1995, Significance of seismic reflections beneath a tilted exposure of deep continental crust, Tehachapi Mountains, California: Journal of Geophysical Research, v. 100, p. 2069–2087, doi: 10.1029/94JB02127.

McDougall, I., and Harrison, T.M., 1999, Geochronology and thermochronology by the ^{40}Ar/^{39}Ar method: New York, Oxford University Press, 269 p.

Mezger, K., Essene, E.J., and Halliday, A.N., 1992, Closure temperatures of the Sm-Nd system in metamorphic garnets: Earth and Planetary Science Letters, v. 113, p. 397–409, doi: 10.1016/0012-821X(92)90141-H.

Naeser, N.D., Naeser, C.W., and McCulloch, T.H., 1990, Thermal history of rocks in southern San Joaquin Valley, California: Evidence from fission-track analysis: American Association of Petroleum Geologists Bulletin, v. 74, p. 13–29.

Niemi, N., Spotila, J., and House, M., 2004, Crustal exhumation in a transpressional setting, San Emigdio Mountains, California: Geological Society of America Abstracts with Programs, v. 36, no. 5, p. 24.

Nilsen, T.H., 1987, Stratigraphy and sedimentology of the Eocene Tejon Formation, western Tehachapi and San Emigdio Mountains, California: U.S. Geological Survey Professional Paper 1268, 110 p.

Nourse, J., 1989, Geology of the Rand thrust complex, part 1 [Ph.D. thesis]: Pasadena, California Institute of Technology, p. 5–63, 2 plates.

Peacock, S.M., 1992, Blueschist-facies metamorphism, shear heating, and *P-T-t* paths in subduction shear zones: Journal of Geophysical Research, v. 97, p. 17,693–17,707.

Pickett, D.A., 1991, An isotopic and petrologic study of an exposure of the deep Sierra Nevada batholith, Tehachapi Mountains, California [Ph.D. thesis]: Pasadena, California Institute of Technology, 272 p.

Pickett, D.A., and Saleeby, J.B., 1993, Thermobarometric constraints on the depth of the exposure and conditions of plutonism and metamorphism at deep levels of the Sierra Nevada batholith, Tehachapi Mountains, California: Journal of Geophysical Research, v. 98, p. 609–629.

Pickett, D.A., and Saleeby, J.B., 1994, Nd, Sr, and Pb isotopic characteristics of Cretaceous intrusive rocks from deep levels of the Sierra Nevada batholith, Tehachapi Mountains, California: Contributions to Mineralogy and Petrology, v. 118, p. 198–205, doi: 10.1007/BF01052869.

Reiners, P.W., Spell, T.L., Nicolescu, S., and Zanetii, K.A., 2004, Zircon (U-Th)/He thermochronometry: He diffusion and comparisons with ^{40}Ar/^{39}Ar dating: Geochimica et Cosmochimica Acta, v. 68, p. 1857–1887, doi: 10.1016/j.gca.2003.10.021.

Ross, D.C., 1979, Summary of petrographic data of basement rock samples from oil wells in the southeastern San Joaquin Valley, California: U.S. Geological Survey Open-File Report 79-400, 11 p., 1 plate.

Ross, D.C., 1983, Generalized geologic map of the southern Sierra Nevada, California, showing the location of samples for which K-Ar radiometric age data and Rb/Sr data have been determined: U.S. Geological Survey Open-File Report 83-231, scale 1:250,000, 1 plate.

Ross, D.C., 1989, The metamorphic and plutonic rocks of the southernmost Sierra Nevada, California and their tectonic framework: U.S. Geological Survey Professional Paper 1381, 159 p., 2 plates.

Rapp, R.P., Watson, E.B., and Miller, C.F., 1991, Partial melting of amphibolite/eclogite and the origin of Archean trondhjemites and tonalites: Precambrian Research, v. 51, p. 1–25, doi: 10.1016/0301-9268(91)90092-O.

Rubin, C.M., and Saleeby, J.B., 1992, Thrust tectonics and Cretaceous intracontinental shortening in southeast Alaska, *in* McClay, K.R., ed., Thrust tectonics: London, Chapman and Hall, p. 407–419.

Ruppert, S., Fliedner, M.M., and Zandt, G., 1998, Thin crust and active upper mantle beneath the southern Sierra Nevada in the western United States: Tectonophysics, v. 286, p. 237–252, doi: 10.1016/S0040-1951(97)00268-0.

Rushmer, T., Antignano, A., IV, and Price, R.P.W., 2003, Melt generation and extraction in the lowermost crust: An experimental test of a natural setting: Geological Society of America Abstracts with Programs, v. 35, no. 6, p. 222.

Saleeby, J.B., 1990, Progress in tectonic and petrogenetic studies in an exposed cross section of young (~100 Ma) continental crust, southern Sierra Nevada, California, *in* Salisbury, M.H., ed., Exposed cross sections of the continental crust: Dordrecht, Netherlands, D. Reidel Publishing, p. 137–158.

Saleeby, J.B., 2003, Segmentation of the Laramide slab—Evidence from the southern Sierra Nevada region: Geological Society of America Bulletin, v. 115, p. 655–668, doi: 10.1130/0016-7606(2003)115<0655:SOTLSF>2.0.CO;2.

Saleeby, J.B., and Busby-Spera, C.V., 1986, Fieldtrip guide to the metamorphic framework rocks of the Lake Isabella area, southern Sierra Nevada, California, *in* Dunne, G.C., ed., Mesozoic and Cenozoic structural evolution of selected areas, east-central California: Geological Society of America Cordilleran Section Guidebook Volume, p. 81–94.

Saleeby, J., and Foster, Z.A., 2004, Fieldtrip guide to study the attenuation and truncation of the southernmost Sierra Nevada batholith, *in* Morris, P., and Ponek, M., eds., San Joaquin Geological Society Field Guide: Bakersfield, California, American Association of Petroleum Geologists Fieldtrip Guide, 28 p., 1 plate.

Saleeby, J.B., and Sharp, W.D., 1980, Chronology of the structural and petrologic development of the southwest Sierra Nevada foothills, California: Geological Society of America Bulletin, v. 91, Part I, p. 317–320, Part II, p. 1416–1535.

Saleeby, J.B., Sams, D.B., and Kistler, R.W., 1987, U/Pb zircon, strontium, and oxygen isotopic and geochronological study of the southernmost Sierra Nevada batholith, California: Journal of Geophysical Research, v. 92, p. 10,443–10,446.

Saleeby, J.B., Kistler, R.W., Longiaru, S., Moore, J.G., and Nokleberg, W.J., 1990, Middle Cretaceous silicic metavolcanic rocks in the Kings Canyon area, central Sierra Nevada, California, *in* Anderson, J.L., ed., The nature and origin of Cordilleran magmatism: Geological Society of America Memoir 174, p. 251–270.

Saleeby, J.B., Ducea, M., and Clemens-Knott, D., 2003, Production and loss of high-density batholithic root—Southern Sierra Nevada, California: Tectonics, v. 22, no. 6, p. 1–24, doi: 10.1029/2002TC001374.

Sams, D.B., and Saleeby, J.B., 1988, Geology and petrotectonic significance of crystalline rocks of the southernmost Sierra Nevada, California, *in* Ernst, W.G., ed., Rubey Volume VII, Metamorphism and Crustal Evolution in the Western United States: Englewood Cliffs, New Jersey, Prentice-Hall, p. 866–893.

Selverstone, J., and Chamberlain, C.P., 1990, Apparent isobaric *P-T* paths from granulites: Two counterexamples from British Columbia and New Hampshire: Geology, v. 18, p. 307–310, doi: 10.1130/0091-7613(1990)018<0307:AICPFG>2.3.CO;2.

Sharry, J., 1981, The geology of the western Tehachapi Mountains, California [Ph.D. thesis]: Cambridge, Massachusetts Institute of Technology, 215 p., 3 plates.

Silver, L.T., Taylor, H.P., Jr., and Chappell, B., 1979, Some petrological, geochemical and geochronological observations of the Peninsular Ranges batholith near the international border of the U.S.A. and Mexico, *in* Abbott, P.L., and Todd, V.R., eds., Mesozoic crystalline rocks: Peninsular Ranges batholith, pegmatites and Point Sal ophiolite: Geological Society of America Annual Meeting Field Trip Guidebook, p. 83–110.

Sisson, T.W., Grove, T.L., and Coleman, D.S., 1996, Hornblende gabbro sill complex at Onion Valley, California, and a mixing origin for the Sierra Nevada batholith: Contributions to Mineralogy and Petrology, v. 126, p. 81–108, doi: 10.1007/s004100050237.

Spear, F.S., 1991, On the interpretation of peak metamorphic temperatures in light of garnet diffusion during cooling: Journal of Metamorphic Geology, v. 9, p. 379–388.

Stern, T., Bateman, P.C., Morgan, B.A., Newell, M.F., and Peck, D.L., 1981, Isotopic U-Pb ages of zircon from the granitoids of the central Sierra Nevada, California: U.S. Geological Survey Professional Paper 1185, 17 p.

Tarduno, J.A., McWilliams, M., Debiche, M.G., Sliter, W.V., and Blake, M.C., Jr., 1985, Franciscan Complex limestones: Accreted remnants of Farallon plate oceanic plateaus: Nature, v. 317, p. 345–347, doi: 10.1038/317345a0.

Tobisch, O.T., Saleeby, J.B., Renne, P.R., McNulty, B., and Tong, W., 1995, Variations in deformation fields during development of a large-volume magmatic arc, central Sierra Nevada, California: Geological Society of America Bulletin, v. 107, p. 148–166, doi: 10.1130/0016-7606(1995)107<0148:VIDFDD>2.3.CO;2.

Todd, V.R., Erskine, B.G., and Morton, D.M., 1988, Metamorphic and tectonic evolution of the northern Peninsular Ranges batholith, southern California, *in* Ernst, W.G., ed., Metamorphism and crustal evolution of the western United States (Rubey Volume VII): Englewood Cliffs, New Jersey, Prentice-Hall, p. 894–937.

Van der Laan, S.R., and Wyllie, P.J., 1992, Constraints on Archean trondhjemite gneiss from hydrous crystallization experiments on Nuk gneiss at 10–17 kb: Journal of Geology, v. 100, p. 57–68.

Watson, E.B., and Harrison, T.M., 1984, Accessory minerals and the geochemical evolution of crustal magmatic systems: A summary and prospectus of experimental approaches: Physics of the Earth and Planetary Interiors, v. 35, p. 19–30, doi: 10.1016/0031-9201(84)90031-1.

White, A.J.R., and Chappell, B.W., 1977, Ultrametamorphism and granitoid genesis: Tectonophysics, v. 43, p. 7–22, doi: 10.1016/0040-1951(77)90003-8.

Wolf, M.B., and Wyllie, P.J., 1994, Dehydration melting of amphibolite at 10 kb: Effects of temperature, time: Contributions to Mineralogy and Petrology, v. 115, p. 369–383, doi: 10.1007/BF00320972.

Wood, D.J., and Saleeby, J.B., 1998, Late Cretaceous–Paleocene extensional collapse and disaggregation of the southernmost Sierra Nevada batholith: International Geological Reviews, v. 39, p. 973–1009.

Wyllie, P.J., and Wolf, M.B., 1993, Amphibolite dehydration melting: Sorting out the solidus, *in* Prichard, H.M., et al., eds., Magmatic processes and plate tectonics: Geological Society [London] Special Publication 76, p. 405–416.

Zen, E-an, 1989, Plumbing the depths of batholiths: American Journal of Science, v. 289, p. 1137–1157.

Manuscript Accepted by the Society 13 July 2006